12-2010

A System for Measuring Radiation Induced Chemical Products in Atmospheric Gases Using Optical Detection Methods

Tyler Webster Reese
University of Southern Mississippi

The University of Southern Mississippi

A SYSTEM FOR MEASURING RADIATION INDUCED CHEMICAL PRODUCTS IN ATMOSPHERIC GASES USING OPTICAL DETECTION METHODS

by

Tyler Webster Reese

A Thesis
Submitted to the Graduate School
of The University of Southern Mississippi
in Partial Fulfillment of the Requirements
for the Degree of Master of Science

Approved:

_____
Director

_____

_____

_____
Dean of the Graduate School

December 2010

ABSTRACT

A SYSTEM FOR MEASURING RADIATION INDUCED

CHEMICAL PRODUCTS IN ATMOSPHERIC GASES

USING OPTICAL DETECTION METHODS

by Tyler Webster Reese

December 2010

This research is a part of an effort to characterize the chemical products generated by radiation interacting with atmosphere. One method of detecting ionizing radiation is to monitor the radiation induced products in the atmosphere around the source. This project explored the potential for using Cavity Ringdown Spectroscopy to evaluate the presence of chemical products generated by the air-radiation interaction near an alpha radiation source. In particular, measurements of ozone concentration within a controlled atmosphere chamber as affected by radiation exposure were obtained.

The first portion of this thesis provides brief reviews of ionizing radiation and ozone formation as well as an explanation of Cavity Enhanced Absorption Spectroscopy and Cavity Ringdown Spectroscopy. This is followed by a description of the optical and vacuum systems that were available and the modifications required to integrate the optical system into the vacuum chamber to achieve the ability to optically monitor the ozone levels in a controlled atmosphere. Both the ringdown data collection and the vacuum system control processes were automated using software developed throughout this project. A discussion of these programs is also included in this thesis. Finally, results are

presented and discussed that verify the system is capable detecting a correlation between the presence of an absorbing species and exposure to ionizing radiation.

ACKNOWLEDGMENTS

The author would like to thank research advisor and thesis director, Dr. Chris Winstead, for providing a project and environment that promoted creativity and curiosity in addition to the collaborative research process that valued student feedback and faculty input equally. I would also like to thank the rest of the committee, Dr. Lawrence Mead and Dr. Michael Vera, for all of their advice and willingness to help throughout this whole process. Special thanks go to Mr. Glenn Messer for his advice as well as donating his time, expertise, and materials in the last minute fabrication of the radiation source holder integral in obtaining the final results discussed in this thesis.

I would like to extend my sincerest thanks and appreciation to my parents whose love and encouragement combined with their ability to listen patiently and/or send me back to work, and the wisdom to know which was needed, helped to keep my head on straight and to keep me pushing forward through this chapter of my life.

TABLE OF CONTENTS

ABSTRACT ……...ii

ACKNOWLEDGMENTS…… .iv

LIST OF TABLES……... .vi

LIST OF ILLUSTRATIONS……... vii

CHAPTER

I. INTRODUCTION ……...1

II. BRIEF REVIEW OF RADIOACTIVE DECAY…… ..3

III. OZONE PRODUCTION ……12

IV. CAVITY ENHANCED ABSORPTION SPECTROSCOPY ……..15

V. EXISTING SYSTEMS TO BE UTILIZED ……...23

Existing Optical System
Existing Vacuum System

VI. SYSTEM MODIFICATIONS …… 28

Optical Cavity Construction Method
Preliminary Light Source System
Light Source Currently Being Utilized
Measurement and Data Collection Devices
Sliding Radiation Source Cover
Flow through Capability

VII. SOFTWARE DEVELOPMENT ……42

VIII. DATA COLLECTION AND RESULTS ……... 49

IX. CONCLUSIONS AND FUTURE WORK …… 54

REFERENCES……56

LIST OF TABLES

Table

2.1 Penetration Depth Comparison For Representative Radiation Sources...11

8.1 The Averaged Ringdown Values Corresponding to Each Phase of the Cycle 50

9.1 Predicted Concentrations Resulting from the Observed Shift in Ringdown Time of Other Potential Products of Ionizing Radiation and Their Absorption Cross Sections 54

LIST OF ILLUSTRATIONS

Figure

4.1 Ozone Absorption Spectrum (reproduced with permission) [11].....16

4.2 Representation of basic absorption principle……17

4.3 Basic representation of the CEAS experimental setup……....18

4.4 CW Red laser diode used to demonstrate intensity build up within the optical cavity..……20

5.1 CEAS system design developed during previous work reassembled with minimal changes as an aid in developing design concepts for this research……..... 23

5.2 Previously developed vacuum system…….……...26

6.1 Custom 8” flanges: Left-interior face. Right-exterior face.……... 29

6.2 Rotary Feedthrough: Side view and End view.……..... 30

6.3 Optical mount slotted brass fittings to be anchored within the chamber... 30

6.4 Fully assembled and installed optical setup in vacuum chamber (External adjustments and Internal Optics on one side)……..... 31

6.5 Diode mount and mirror assembly……..... 32

6.6 External Optics Bracket: with and without diode system installed..……33

6.7 Nd:YAG laser and optical components that guide the laser pulses into the optical cavity……....35

6.8 PMT Assembly……...36

6.9 Pneumatic Linear Feedthrough before installation (above) and Linear Feedthrough after installation with pneumatic control lines and solenoid control valve (below).……38

6.10 Sliding aluminum source cover shown opened (left) and closed (right)… 39

6.11 ^{210}Po Sources in the Aluminum Holder.……...40

6.12 Flange allowing flow output from chamber with redundant shut off valve (shown with shut off valves closed)…… 41

7.1 The front panel for Ringdown Alignment Assist.vi (above) displays the user interface, and the corresponding block diagram (below) is an example of the LabVIEW programming language.……... 44

7.2 Front Panel for Ringdown Time.vi with representative data displayed….. 46

7.3 Front Panel for “Cycle Control.vi.”…….…… 47

7.4 Front Panel for “Basic Control.vi.”…… 48

8.1 The plot above shows ringdown time vs elapsed as affected by pressure changes.…… 49

8.2 Demonstrating the ringdown system’s ability to accurately measure O_3.. 51

8.3 Ringdown times vs elapsed time (top) and ppb of o_3 vs elapsed time (bottom) as affected by uncovering and covering the alpha sources.…... 53

CHAPTER I

INTRODUCTION

It is a common understanding that nuclear radiation can be harmful, but when it comes to determining whether there are harmful levels of radioactivity present, current detection devices must interact directly with the radiation. This means that the individual operating the equipment is at risk of being exposed to potentially harmful radiation. This research is a part of exploring the potential for alternative methods of detecting radioactive materials from safer distances.

Similar to the way particles that are produced by radioactive decay interact with conventional radiation detectors, those particles also interact with the atmosphere around them. This atmospheric interaction initiates various chemical reactions and can generate a variety of chemical products. The goal of this research was to design and implement a system that is capable of using Cavity Enhanced Absorption Spectroscopy (CEAS) to detect those chemical products. For this research, ozone was chosen as the target species to monitor.

The chemical products and the rates at which they are created are obviously dependent on which species are available to interact with the radiation. This means that reaction products are directly related to atmospheric composition. Because of this relation, it was necessary to integrate the optical cavity for CEAS into a system that can reliably and precisely control atmospheric conditions. An automated vacuum system that has this capability was available and was chosen to be the mechanism to control the atmospheric conditions during this research. This thesis will include a brief review of radioactive decay, a

discussion of the processes responsible for ozone production in general and in the case of ionizing radiation, an explanation of CEAS, an explanation of the methods used in this research to optically evaluate concentration, and the development of the equipment capable of evaluating the ozone concentrations expected to be produced by an alpha source within a controlled volume as well as the software developed to aid in making these measurements. These efforts are intended to extend the capabilities of the system and to allow for real-time measurements of chemicals produced by a radioactive source via CEAS.

CHAPTER II

BRIEF REVIEW OF RADIOACTIVE DECAY

Discovered in 1896 by Henri Becquerel, radioactive decay is the spontaneous decay of an atomic nucleus through emission of a high-energy particle and/or electromagnetic wave [1]. Not all elements are radioactive nor are all isotopes of a known radioactive element radioactive. Radioactive nuclei are those that through decay lower their energy, meaning a nucleus that is already in its lowest energy state would have no reason to decay. In some cases the radioactive nucleus decays into yet another unstable species that then undergoes another decay until through this process a stable nucleus is reached. The subsequent nuclei are known as daughter nuclei.

Because of the spontaneity of radioactive decay, one cannot predict precisely the time between individual decays or the exact time at which decay will occur. However, it does occur consistently enough that over a sufficiently long time period an average decay rate can be observed. The Becquerel, Bq, is a unit of radioactivity that is equal to one decay per second (s^{-1}). This unit is often much too small for practical application. A slightly more manageable unit is the Curie, Ci, and is equal to $3.7x10^{10}$ decays per second or 37 GBq. The rate of decay of an isotope is directly related to the number of atoms present by the following expression:

$$-dN/dt = \lambda N$$

where N is the number of radioactive atoms present, t is time, and λ is a decay rate constant. Through integration this equation becomes the more familiar:

$$N = N_0 e^{-\lambda t} \quad (2.1)$$

where N_0 is the initial number of radioactive atoms present, and N is the number left at time t. Rearranging this equation allows one to obtain an expression for the commonly used term known as the half life, $t_{1/2}$. The half life is the time it takes for the number of atoms remaining to equal half of the initial amount:

$$\frac{1}{2} = N/N_0 = \exp(-\lambda t_{1/2})$$

$$\therefore \; t_{1/2} = \ln(2)/\lambda \quad (2.2)$$

Because the level of radioactivity is directly proportional to the amount of material present, the half life is also equal to the time it takes for the activity level due to a particular isotope to reduce by a factor of one half. Accordingly, if one is provided with the initial activity level, the half life, and when the initial measurement was made for a given radioactive sample, one is able to calculate the current activity level for that sample [2].

Commonly discussed decays include alpha particle (α), beta particle (β), and gamma ray (γ) emissions. These emissions all fall into the category of ionizing radiation. This means that they carry enough energy and are sufficiently capable of interacting with the electrons in the surrounding material to ionize them. Some radiation detection methods utilize this process directly to measure the presence of radioactive decay. A small cathode/anode tube filled with gas is exposed to radiation. When a gas molecule is ionized, the freed electron is attracted to the anode, and a small current can be measured. The larger the current, the more frequently ionization is occurring which indicates a higher flux of radiation through the detector. Each type of radioactive emission has different

physical characteristics and accordingly interacts with the surrounding material with different levels of efficiency.

In some cases, after a nucleus decays via alpha or beta decay, the daughter nucleus is produced in an excited state. Gamma radiation is one method for the excited nucleus to release that extra energy. Because this emission results from a transition between energy levels in the nucleus, the photons produced by an element undergoing gamma emission have a very narrow line width of energies. Gamma radiation does not change the nucleus' mass or charge. It is not a heavy or charged particle; it is a photon that has no mass. Because of the relatively high energies associated with a gamma photon, the probability for it to interact with matter is limited, and this results in a very long mean free path. There are three ways that gamma ray energy can be dissipated: Compton scattering, photo ionization (photoelectric effect), and pair production. When Compton scattering occurs, the gamma ray transfers enough of its energy to an atom or molecule to eject an electron, and a gamma ray with energy equal to the original gamma ray energy minus the binding energy and kinetic energy of the ejected electron continues to propagate. The photoionization process is similar to Compton scattering except that any excess energy from the incident gamma ray is transferred to the electron as kinetic energy. No lower energy photon in produced. Pair production is the process of converting energy to mass in the form of an electron-positron pair. An electron and a positron each individually have a rest mass of .51 MeV. Therefore, pair production can only occur with gamma rays that have energy greater than or equal to 1.02 MeV, and

any excess energy is carried away as kinetic energy. In general it has been observed that gamma rays with lower energies are more likely to be absorbed through photoionization. Intermediate energy gamma rays are more likely to dissipate energy through Compton scattering, and higher energy gamma rays have a higher probability of pair production. Gamma radiation can also interact with surrounding matter without dissipating energy through Rayleigh scattering. Each of these four processes has a certain probability of occurring that is a function of the incident gamma ray energy and parameters of the material with which it interacts (composition, density, etc.). Calculations and experimental measurements have been made that account for the cumulative effect of these processes for a given set of conditions to provide information concerning the overall dissipation of radiation.

$$I = I_0 e^{-\mu x} \tag{2.3}$$

where I_0 is the initial intensity, μ is calculated from (μ/ρ) which is known as the mass attenuation coefficient with units cm^2/g and is determined by the material the gamma ray is traveling through, x is the linear distance from the source, and I is the intensity at distance x. In the mass attenuation coefficient term, the value ρ is the density of the material, and 1/μ is the distance from the source that I is reduced to $I_0 e^{-1}$ [2].

Beta particles are electrons emitted when a neutron decays into an electron and a proton. The proton remains in the nucleus while the electron is ejected as the beta particle. This method of decay decreases the mass of the nucleus by the mass of the emitted electron plus its binding energy and leaves

the nucleus with a Z+1 charge. An anti-neutrino is also emitted during beta decay, and while its rest mass is not significant when compared to the proton, neutron, or even electron mass, it is able to account for significant amounts of energy via its kinetic energy. The binding energy released during beta decay is carried away as kinetic energy by the beta particle and the anti-neutrino. These particles can scatter at a variety of angles with the beta particle and anti-neutrino each carrying away some portion of the excess energy. Through relatively simple conservation laws, it can be seen that for each beta emitter this allows the beta particle energy to fall into a broad band of energies up to some maximum value. This is in contrast to gamma emitters that only emit gamma rays at a specific energy. Being a charged particle allows beta radiation to interact directly with matter through collisions. Its mass is very small (9.11×10^{-31} kg), and this has two notable affects on its behavior. To carry away any appreciable amount of energy, it must be moving at very high velocities. While it does not penetrate as deeply as a gamma ray does, this does allow it to cover a relatively large distance before it loses all of its energy. The other significant effect of the beta particle's size comes from the fact that it is colliding with other electrons of equal mass. As it ionizes the surrounding material, it is scattered over very large angles due to these equal body collisions. In denser materials, the beta particle also loses a small amount of energy through interactions with the positive electric fields created by the nuclei near its path. As these fields slow the beta particle, electromagnetic radiation is emitted known as bremsstrahlung radiation. While this is still possible in a gas, the reduced probability of this occurring indicates

that it will not be a significant source of energy loss compared to electron collisions. Similar to gamma rays, calculations have been made that approximate the average penetration depth of a beta particle along its initial direction in a given material. Instead of being an equation for intensity however, a simple range is calculated for a beta particle with a given initial energy in a particular material, given in g/cm^2. Dividing that value by the actual density of the material in question, in g/cm^3 provides an average depth in cm. While there are certain to be variations in penetration depth from one beta particle to another, and beta particles from the same source do not all have the same energy, this average range provides a very good idea of the distance one would expect a large portion of beta radiation to reach [2].

Alpha particles are composed of two protons and two neutrons. After alpha emission, the nucleus mass is decreased by approximately four atomic mass units (amu) and has a remaining charge of Z-2. Similar to gamma radiation, all of the alpha particles emitted by a particular element have very nearly the same energy. Compared to beta radiation, alpha particles move at much slower velocities due to their large mass. Given their large size and double charge, alpha particles are still very effective ionizers. Alpha particles dissipate their energy via collisions. Alpha particles are also much less susceptible to scattering and changes in direction due to their massiveness compared to the orbital electrons with which they collide. They do still scatter slightly due to Coulomb field interactions with the positively charged nuclei, but the effect is much less than occurs with beta particles. As with the beta particles, one can find tables of

average ranges for a specific material, again given in g/cm^2 to be divided by the actual density of the material, that provide an approximate penetration depth that accounts for energy loss due to collisions and any scattering that may occur [2].

As an example and to demonstrate why the radiation sources used in this research were chosen, range calculations for dry air near sea level for three different sources are provided. Three potential sources available for this type of work are ^{60}Co, ^{90}Sr, and ^{210}Po. Cobalt-60 undergoes a beta decay into Nickel-60 which then undergoes a coincident gamma-gamma decay producing two gamma rays: one with 1.1732 MeV of energy, and one with 1.3325 MeV of energy. Strontium-90 undergoes beta decay into Yttrium-90 that has a sufficiently short half-life to immediately undergo a second beta decay and a gamma emission into Zirconium-90. The maximum beta particle energies for each are 0.546 MeV and 2.28 MeV respectively. Polonium-210 is a pure alpha emitter with an alpha energy of 5.3 MeV. The density of dry air near sea level is 1.20479×10^{-3} g/cm^3 [3]. This value will be used for all of the following penetration depth calculations.

The mass attenuation coefficients, (μ/ρ), available for gamma rays in dry air are not listed in high enough resolution to find them for gamma energies 1.1732 MeV and 1.3325 MeV, but the value listed for a 1.25 MeV gamma ray will provide adequate information to provide an estimate of how far these gamma rays would travel before depositing their energy into a system. The dry air coefficient provided for a 1.25 MeV gamma ray is 5.687×10^{-2} cm^2/g [4]. $1/\mu$ provides the distance at which one can expect to find the gamma intensity reduced by a factor of 1/e meaning that there would be approximately 36.79% of

the initial gamma radiation present at that distance.

$$(\mu/\rho)*(\rho) = (5.678\text{x}10^{-2}\ cm^2/g)*(1.20479\text{x}10^{-3}\ g/cm^3)$$

$$\mu = 6.841\text{x}10^{-5}\ cm^{-1}$$

$$1/\mu = 1.462\text{x}10^{4}\ cm$$

$$1/\mu = 146.2\ m$$

Therefore, the ^{60}Co gamma rays would be expected to travel well over 100 m in air.

The beta energy values nearest 0.546 MeV and 2.28 MeV that have range values available are .550 MeV and 2.50 MeV. The corresponding range values are $2.274\text{x}10^{-1}\ g/cm^2$ and $1.374\ g/cm^2$, respectively [3]. The average penetration depths for these beta particles given that the particles have the maximum available energy are given by:

$$(2.274\text{x}10^{-1}\ g/cm^2)/(1.20479\text{x}10^{-3}\ g/cm^3) = 1.887\text{x}10^{2}\ cm$$

$$= 1.887\ m$$

and

$$(1.374\ g/cm^2)/(1.20479\text{x}10^{-3}\ g/cm^3) = 1.140\text{x}10^{3}\ cm$$

$$= 11.40\ m$$

This indicates that beta particles from ^{90}Sr travel several meters in air before dissipating they energy.

The alpha energy nearest to 5.3 MeV that has a provided range value is 5.5 MeV. The range value for a 5.5 MeV alpha particle is $5.048\text{x}10^{-3}\ g/cm^2$ [3]. The average penetration depth for these alpha particles is:

$$(5.048\text{x}10^{-3}\ g/cm^2)/(1.20479\text{x}10^{-3}\ g/cm^3) = 4.190\ cm$$

Table 2.1 Penetration Depth Comparison for Representative Radiation Sources

Radiation Type	Source	Energy Values of Emitted Radiation (MeV)	Nearest Energy Value with Mass Attenuation Provided (MeV)	Expected Range (m)
Gamma	^{60}Co	1.17 1.33	1.25	146.2*
Beta	^{90}Sr	0.546	0.55	1.89
		2.28	2.5	11.4
Alpa	^{210}Po	5.3	5.5	0.042

*Gamma range corresponds to disctance at which the intensity is expected to be reduced by a factor of 1/e

The apparatus available for this project to contain the components of this experiment including the radioactive source and the gases intended to interact with the emitted radiation is an 18” (45.72 cm) diameter spherical vacuum chamber. From these calculations, summarized in the chart above, it can be seen that neither a beta particle nor a gamma ray would have deposited a significant fraction of its energy into the surrounding gases before it reached the chamber wall. An alpha particle from ^{210}Po on the other hand transfers all of its energy through ionization well before it can reach the chamber wall. This was the main reason a ^{210}Po source was selected for this research. The ^{210}Po source deposits the radiation energy in a small volume leading to a higher density of chemical reactants than would be possible for a beat or gamma source of similar activity.

CHAPTER III

OZONE PRODUCTION

The chemical processes that produce ozone (O_3) in the upper atmosphere have been studied for many years, but upper atmospheric chemistry remains an active area of research. The predominant method of ozone production is through the reaction of molecular oxygen (O_2) with atomic oxygen (O) with a third body (M) present to carry away excess energy:

$$O_2 + O + M \rightarrow O_3 + M \quad (3.1)$$

Because the atmosphere is mainly comprised of molecular nitrogen (N_2) and O_2, one of these molecules is most often the third body present to carry away the energy released by the reaction. Electromagnetic radiation of wavelength $\lambda <$ 240 nm has sufficient energy to dissociate O_2 [5]. In the upper atmosphere, there is still enough sunlight at these wavelengths to produce a large quantity of oxygen atoms. While there are a limited number of competing reactions, a significant amount of O_3 is produced in the upper atmosphere. There have been several measurements of O_3 in the upper atmosphere verifying its presence, but it is also evident from its effect on the solar irradiation that reaches the Earth's surface. Ozone is a very strong optical absorber from wavelengths 210 nm to 310 nm, known as the Hartley Band [5], and the absence of this light in the lower atmosphere is another indication of significant amounts of ozone in the upper atmosphere.

O_3 production processes in the lower atmosphere resulting from chemical byproducts of smog have also been studied. In a study that observed various

pollutant levels during a 24-hour period in Los Angeles, CA, it was verified that in addition to the carbon monoxide (CO) produced by incomplete combustion, nitric oxide (NO) was also produced during the initial pollutant spike that corresponded with the morning rush hour. Over a period of a few hours a significant portion of this NO is converted into nitrogen dioxide (NO_2) [6][5]. The presence of NO_2 also makes O_3 production possible. NO_2 photodissociates when irradiated with light with wavelengths shorter than 400nm according to the follow process

$$NO_2 + h\nu \rightarrow NO + O \qquad (3.2)$$

where $h\nu$ represents the energy from the $\lambda<400$ nm photon [5]. This production of free oxygen atoms is what allows for the production of O_3 from automobile emissions in the lower atmosphere. It was also noted that there was not an O_3 level increase that correlated with the evening rush hour. This fact reinforces the need for the photodissociation of NO_2 as a precursor for O_3 generation from lower atmosphere pollution [5].

There have also been a number of studies of the chemical effects of radiation on air-like mixtures. Many of them utilize a high energy electron beam to simulate a beta radiation source. Some of the earlier studies used chemiluminescence to measure the chemicals produced when flowing N_2-O_2 mixtures were exposed to radiation [7]. Some more recent studies using both N_2-O_2 mixtures and pure O_2 employed methods of alternating exposure to radiation and infrared absorption spectroscopy to measure chemical levels [8] or a UV absorption method to measure O_3 as well as a chemical detection method to measure other products generated [9]. These methods all confirmed the

production of O_3 as well as many other products including NO, NO_2, N_2O, NO_3, and N_2O_5. There were also studies done that included water vapor (H_2O) and found that free hydrogen (H) atoms dissociated from the H_2O allowed for production of a number of acids that were in turn responsible for catalyzing the production of nitrogen-oxygen combinations [10]. This research differs from other studies in that measurements are taken on a time scale comparable to that of the generation of the chemical products from the air-radiation interaction. Measurements are continuously collected as a function of exposure time. This will ultimately allow for more direct characterization of the chemical kinetics associated with radiation-air interactions. For the time being, until a more thorough understanding of the kinetics involved is available, it will be assumed that a process similar to that which occurs in the upper atmosphere is taking place in the presence of radiation, and through interaction with the radiation, free oxygen atoms are produced that are then able to interact with O_2 to generate O_3.

CHAPTER IV

CAVITY ENHANCED ABSORPTION SPECTROSCOPY

Absorption spectroscopy uses the fact that each atom and molecule interacts differently with electromagnetic radiation. It can be used to identify which atomic or molecular species is present and in some cases how much of a particular species is present. Atoms and molecules all have a variety of excitable electronic states, and molecules are also capable of mechanical excitation (twisting, bending, compressing, rotating, etc.). These states allow absorption of photons whose energies match the excitation energies. An atom or molecule's ability to absorb photons over a variety of wavelengths is referred to as its absorption spectrum. Because different atomic and molecular species have different numbers of electrons and protons as well as, in the case of molecules, different physical configurations, each absorption spectrum has a unique profile that can serve as a finger print for that particular atom or molecule. Below is the absorption spectrum for Ozone. The names on the chart reflect the discoverer of the particular bands.

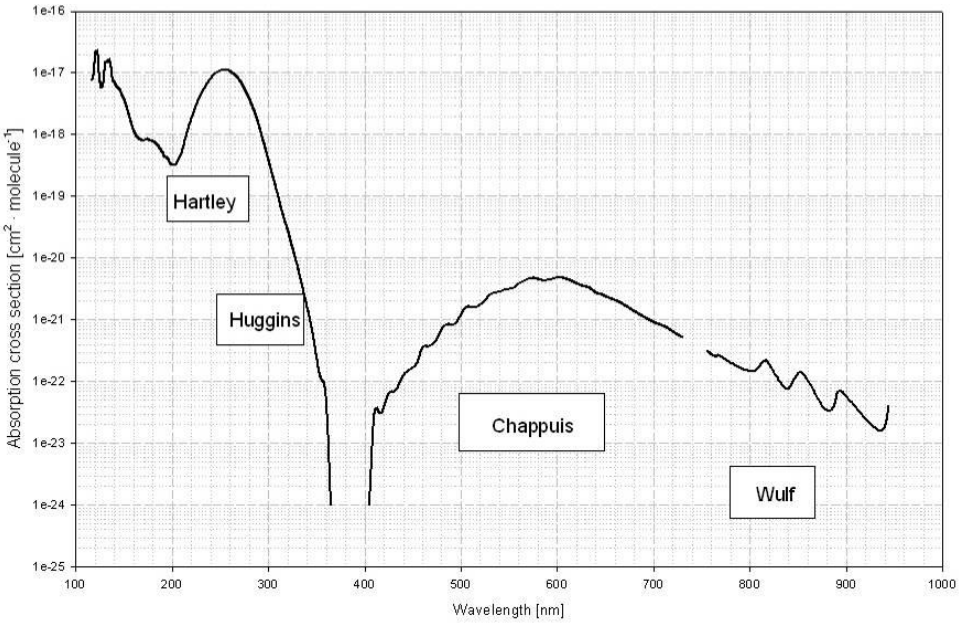

Figure 4.1 Ozone Absorption Spectrum (reproduced with permission) [11].

A species' ability to absorb a particular wavelength of light is quantified by the absorption cross section at that wavelength. The peaks in spectra indicate wavelengths that are more strongly absorbed while the wavelengths with smaller absorption cross sections are not absorbed strongly. The units of absorptions cross section are given in cm^2/molecule. With a larger number density or a longer opportunity for the light to interact with the absorber, more light will be absorbed. This can be described using Beer's Law:

$$I(x, \lambda) = I_0 e^{-\alpha(\lambda)x} \qquad (4.1)$$

$$\text{given } \alpha(\lambda) = \sigma(\lambda)N$$

where I is the detected intensity, I_0 represents the initial incident intensity of electromagnetic radiation of wavelength λ, e is the base of the natural logarithm, x is the distance traveled by the light in the presence of the absorber measured in meters, and α(λ) is the attenuation coefficient which is equal to the product of

the absorption cross section, σ(λ), in meters^2 and the number density of the absorber, N, in number per meter^3 [12,13,14].

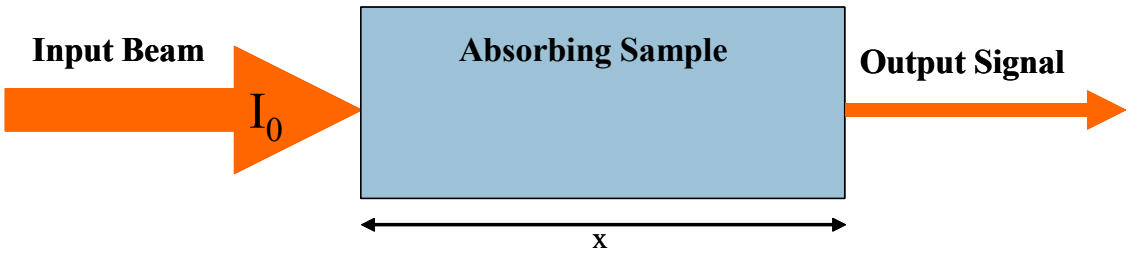

Figure 4.2 Representation of basic absorption principle.

One general method of absorption spectroscopy is to expose an unknown sample to a continuous distribution of light. By scanning the transmitted light one wavelength at a time and comparing incident intensity to transmitted intensity, one could use Beer's Law to quantitatively construct the absorption spectrum for the sample over the wavelengths scanned, allowing it to be compared to known spectra. Methods like this initially only provide information concerning what may be present in an unknown sample. However, once the absorber is identified, using a known absorption cross section and Beer's law one would then be able to calculate the number density of the absorber.

One does encounter a problem with making reliable measurements for absorbers with weak cross sections or in trace concentrations. Under these conditions the change in intensity from absorption may not be significant enough to accurately make measurements. From Beer's law, it can be seen for such cases that the only way to increase the effect of absorption is to increase the distance the light travels through the absorbing medium. Cavity enhanced absorption spectroscopy (CEAS) is used to create greatly increased effective

path lengths within the laboratory environment.

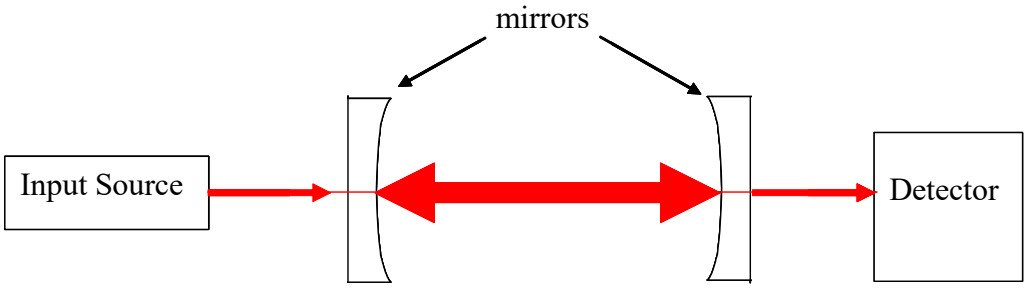

Figure 4.3 Basic representation of the CEAS experimental setup.

CEAS employs two or more mirrors to trap the incoming light and repeatedly redirect it back through the absorbing sample thus providing an extended opportunity for absorption to occur. The optical cavity utilized in this research was created by two spherical mirrors separated by a distance, d, assumed to have equal reflectivity, R, and both transmit a small percentage, T. Both R and T are a function of wavelength. Aligning the mirrors such that the light does not diverge out the sides of the cavity is the condition that produces the greatly increased effective path length. However, it is not an entirely lossless system. Each time the light is reflected a small portion is transmitted through the mirror and the light remaining within the cavity is reduced by a factor of R. For the light to reach a detector on the other side of the optical cavity, the light must pass through the mirror nearest the light source on the way in and through the far mirror on the way out which results in an overall reduction in intensity by a factor of T^2. Therefore, light making one round trip before reaching the detector experiences an overall intensity reduction by a factor of T^2R^2 in addition to doubling the length over which absorption occurs:

$$I = I_0 T^2 R^2 e^{-\alpha(\lambda)2d}. \quad (4.2)$$

After making n round trips within the cavity, the intensity is reduced by a factor of T^2R^{2n}. Putting this in equation (4.2) and rearranging slightly yields

$$I = I_0 T^2 R^{2n} e^{-\alpha(\lambda)2nd} \quad (4.3)$$

$$I = I_0 T^2 e^{2n\ \ln(R)} e^{-\alpha(\lambda)2nd} \quad (4.3b)$$

When an absorbing sample is not present, the second exponential term vanishes, and intensity loss within the cavity is due solely to loss during reflections. Rearranging equation (4.3) to include the first exponential term shown in (4.3b) allows one to recognize that when the intensity drops to a value

$$I = I_0 T^2 (1/e),$$

$$\text{then} \quad 2n\ \ln(R) = -1.$$

This means that the number of round trips made before the light inside a cavity without an absorbing sample is reduced by 1/e depends only the reflectivity of the mirrors:

$$n = -1/(2\ln(R)). \quad (4.4)$$

For example, in a cavity with 99.7 % reflective mirrors separated by a distance of 50 cm, the number of round trips made before the intensity is reduced by a factor of 1/e is approximately 166 round trips. Given that the length of one round trip is 2nL, the distance traveled by the light in 166 round trips would be 166 m. In a cavity created by mirrors with 99.9% reflectivity, the number of round trip is increased to approximately 499.7 which would correspond to an effective path length of nearly 500 m. Mirrors are available with reflectivity values in excess of 99.99% which would extend the path length to nearly 5000 m making

almost 5000 round trips.

There are many different methods that utilize the basic principles of CEAS. The method employed for this research was cavity ringdown spectroscopy (CRDS) using a laser as the light source. In this method, rather than measuring intensity, the time response of the light in the cavity is determined. For a continuous wave (CW) laser with the mirrors aligned so that the incident beam and the reflected light within the cavity are along the same axis, the light from the input source builds up within the optical cavity as can be seen in the picture below.

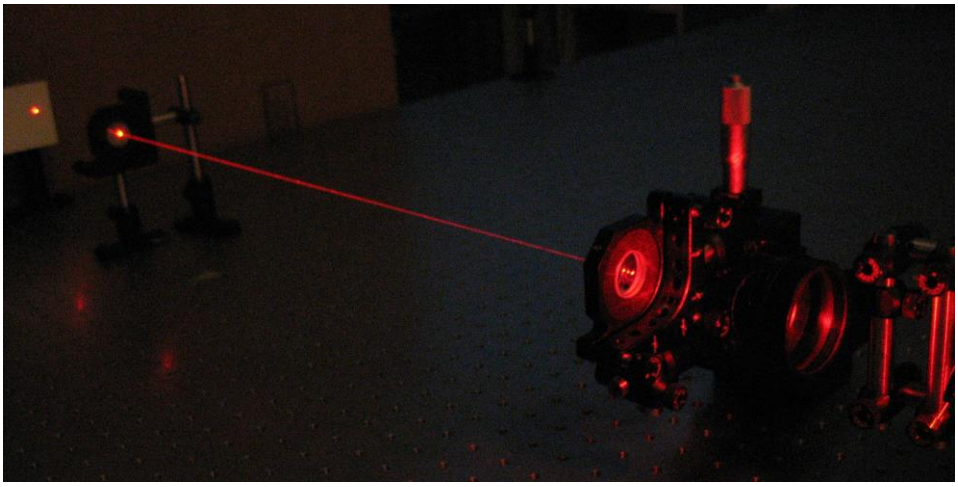

Figure 4.4 CW Red laser diode used to demonstrate intensity build up within the optical cavity.

This internal build up also correlates to the cavity output intensity increasing until it is equal to the input intensity. Build up like this only occurs with continuous wave input sources. In continuous wave CRDS measurements, when this output intensity reaches a desired level, the input source is triggered off, and the intensity in the cavity decays as the light leaks through the mirrors. This results in

an exponential decay of the transmitted intensity. For pulsed input sources, the pulse duration is the limiting factor in the cavity build up and output intensity. Once the input source has stopped pumping the cavity, the cavity output again dies off with an exponential decay. The rate of this decay depends on mirror reflectivity, mirror separation distance, and concentration of an absorbing sample.

An equation for this exponential decay can be reached from equation (4.3b) by recognizing that the time it takes for light to travel n round trips between the cavity mirrors is equal to the separation distance, d, times 2n divided by the speed of light, c:

$$t = 2nd/c, \text{ or}$$

$$t(c/2nd) = 1. \qquad (4.5)$$

Grouping the exponential terms from equation (4.3b) and inserting the expression on the left side of (4.5) yields the following equation:

$$I = I_0 e^{2n\,[\ln(R)-\alpha(\lambda)d](tc/2nd)}$$

$$I = I_0 e^{t\,[\ln(R)-\alpha(\lambda)d](c/d)} \qquad (4.6)$$

$$\text{or} \quad I = I_0 e^{-t/\tau} \qquad (4.7)$$

$$\text{with } 1/\tau = c[-\ln(R)+\alpha(\lambda)d]/d. \qquad (4.8)$$

It should be noted that because CRDS is interested solely in the time dependence of the cavity output and the input intensity is not measured, the T^2 factor is no longer inherently useful and is assumed to be a part of I_0 in this equation. This introduces the value τ which is known as the cavity ringdown time. The ringdown time is equal to the time it takes after the input source stops for the

output intensity to be reduced by a factor of 1/e. This is also used to identify the characteristic ringdown time, τ_0. This value corresponds to the time it takes for loss through the mirrors (i.e., no absorbers) to reduce the output intensity by a factor of 1/e:

$$1/\tau_0 = c[-\ln(R)]/d. \quad (4.9)$$

It is at this point that the reflectivity of the mirrors can be identified

$$R = \exp[-d/(c\tau_0)]. \quad (4.10)$$

With an absorbing sample present, the ring down time represents a combination of light being absorbed and leaking out with each pass. To calculate the number density of an absorbing sample, one takes the difference between equations (4.8) and (4.9).

$$1/\tau - 1/\tau_0 = c\alpha(\lambda) = c\sigma(\lambda)N$$

$$[1/c\sigma(\lambda)][1/\tau - 1/\tau_0] = N \quad (4.11)$$

From this point, the number density N can be converted to parts per million (ppm) or parts per billion (ppb). Using the ideal gas law, pV = NkT, one can calculate the expected number of total molecules per unit volume. Once this number has been calculated, dividing the measure number density of the absorber by the calculated total number density and multiplying by $1x10^6$ for ppm or $1x10^9$ for ppb becomes a simple conversion.

CHAPTER V

EXISTING SYSTEMS TO BE UTILIZED

Prior to this research, there had been projects in the laboratory that involved both O_3 concentration measurement via CEAS and indirect radiation detection. These projects were developed separately, and the focus of this research was to explore the possibility of employing the CEAS O_3 measurement as another method of characterizing radiation-air interactions.

Existing Optical System

The optical system originally developed for O_3 CEAS, shown below, utilized a diode laser, apertures to shape the input beam, an optical cavity built into the ends of a Teflon flow chamber, a microscope objective to focus the cavity output onto the detector face, a photo diode detector, and an oscilloscope [15].

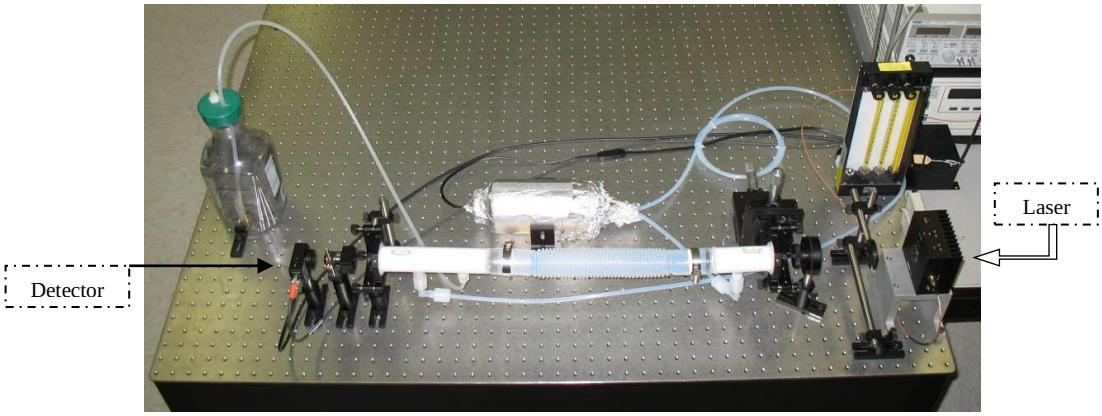

Figure 5.1 CEAS system design developed during previous work reassembled with minimal changes as an aid in developing design concepts for this research.

A photomultiplier tube (PMT) was also used for some measurements in which case the focusing optic was removed as the PMT had a larger reactive surface, and a high intensity pin point image runs the risk of saturating a particular area on the PMT face and giving inaccurate measurements or even damaging the

PMT. The diode laser mount included a focusing optic which aided in shaping the input laser beam; it also had user defined temperature and driving current controls to prevent the laser diode output wavelength from drifting.

Also pictured behind the optical system are a multi-tube flow regulator and a mercury lamp contained within a Teflon bottle wrapped in foil to block the UV emission from the lamp. The flow regulator was used to create controlled mixtures of N_2 and air that were then directed through the bottle exposing them to UV light produced by the mercury lamp, thus generating O_3. Varying the amount of air in the mixture effectively varied the amount of O_2 and in turn controlled the amount of O_3 produced. The resulting mixture was then passed through the ringdown cavity via the flow chamber. A small portion of the gas sample being measured was pulled into a commercial O_3 analyzer to confirm the accuracy of the CEAS measurement. This rest of the gas sample was exhausted through a bottle filled with steel wool to scrub the O_3 and prevent emission into the room. All tubing used to handle the O_3 mixture was also made of Teflon which does not react with O_3 and prevented loss of O_3 due to material interaction. Teflon components also ensured that material degradation would not become a problem after prolonged exposure. This method of measuring O_3 was proven viable, and the initial objective of the research described in this thesis was to design a system capable of integrating this optical system into the existing vacuum chamber system.

Existing Vacuum System

The existing vacuum system was created as a means to explore radiation

induced fluorescence [16] and is still being utilized to further understand this phenomenon. It was also designed to be able to accommodate a variety of other capabilities while maintaining minimal interference on existing configurations. With future work in mind, this system was built with the capabilities of simulating various atmospheric conditions in mind. Versions of the following description have appeared in the proceedings from the 55th International Instrumentation Symposium, a conference sponsored by the Aerospace Industries, Test Measurement, and Process Management and Control Divisions of the International Society of Automation (ISA), and the 2009 ISA Expo. As the presenting author and having retained copyright privileges, it is reproduced here with minimal revisions [17].

Physical Characteristics

The vacuum system utilizes a spherical chamber that is 18 inches in diameter with nineteen circular access ports of varying flange sizes ranging from 2 ¾ to 8 inches; each of these ports has its central axis aligned with the center of the chamber. Five of these ports are used for measuring various parameters of the chamber such as pressure, temperature, and humidity. Two of them have valves attached to them to expose the chamber to two different vacuum pumps. One of the ports has a vent valve that equalizes the chamber pressure with ambient atmosphere, another has a sealable hinged door mounted to it, and a third is attached to a valve system opening to a controlled manifold that can supply precise gaseous mixtures. This manifold has three independently controlled gas introduction valves allowing for sequential introductions of precise

partial pressures of multiple gasses. Of the remaining nine available ports, six opposing ports have been maintained clear of other devices for use as optical axes. One of these optical paths is already in use for the fluorescence detection system. The optical cavity system designed for this research uses the opposing 8” ports to gain the necessary line of sight through the chamber.

Figure 5.2 Previously developed vacuum system.

Pumping Mechanisms

There are three vacuum pumps used in the vacuum system: two mechanical rotary vane pumps and one diffusion pump. The mechanical pumps are connected to angle valves that are used to isolate them from system when not in use. One valve is connected directly to the chamber and the other is connected to the foreline of the diffusion pump. The diffusion pump is connected to a gate valve, which separates the pump from the 8” port on the bottom of the chamber. The mechanical pumps evacuate the majority of the gasses at pressures above the millitorr range, and once the chamber is below 200 mTorr,

the diffusion pump is turned on to bring the system down to high vacuum pressures in the μTorr range.

Chamber Measurement Capabilities

The chamber pressure, temperature, and humidity can be directly measured. An electric feedthrough is attached to two hygrometers operating to measure relative humidity and provide a redundant measurement. A thermocouple feedthrough flange allows for temperature measurements of various aspects of the chamber interior including chamber wall and internal atmospheric temperatures. Two capacitance manometers measure pressures from 1000 to 1 and 1 to .001 Torr respectively, and an ion gauge typically measures pressures below .500 Torr and is capable of measuring down to 1.0×10^{-10} Torr. However, the ion gauge was unavailable for use during this research. Pressure, temperature, and humidity can all be displayed on a push button control panel located on the front of the cart as well as sent to a computer to be read and/or recorded.

System Control

The entire system is monitored and operated by an automated controller. The system has a push button panel that allows a user to manually interact and operate the vacuum system controller. The user also has the ability to access the controller via a graphical user interface (GUI), which was written to allow system interaction from a desktop computer connected to the system via Ethernet cable.

CHAPTER VI

SYSTEM MODIFICATIONS

To take advantage of the vacuum system's ability to create and maintain an isolated atmosphere for CRDS measurements, the vacuum system had to be modified to accommodate the optical cavity. The modification to make a CRDS system capable of evaluating chemical concentrations within the chamber must maintain the ability to adjust the mirror alignment from outside the chamber. The system must also maintain both mechanical stability and utilize a sufficiently stable laser to be able to evaluate concentrations at near ppb levels. There must also be a method of controlling radiation exposure to allow for an accurate τ_0 measurement and allow for accurate evaluation of the time scale of the simulated atmosphere's response to radiation exposure.

Optical Cavity Construction Method

A version of the following was also included in the previously mentioned conference proceedings as part of a preliminary report of the implementation of an optical cavity within a vacuum chamber [17].

While considering potential methods for installing an optical cavity, it must be recognized that any optical element located between the cavity mirrors causes a very significant optical loss. More specifically, if the cavity mirrors were positioned outside the chamber, the vacuum viewports would be located within the cavity. The light circulating in the cavity would be deflected out of the cavity, causing extreme loss and preventing CRDS measurements. Some possible methods for including adjustable mirrors in a vacuum system include mounting

the mirrors on vacuum bellows or mounting the mirror on a large o-ring. Both of these methods behave similar to the Teflon flow chamber with the cavity mirrors built into the chamber walls. Vacuum bellows remain somewhat flexible at vacuum pressures and allow for adjustments. Alternatively a thick o-ring would allow for the use of mounting screws to press the mounted mirror into the o-ring compressing it and adjusting the angle of the mirror. Unfortunately, o-rings do not reliably hold a seal at the pressure maintained in the chamber. Most significantly, both of these methods would allow the cavity to expand and contract slightly as the pressure inside the chamber was varied. This expansion and contraction compromises the optical alignment of the cavity.

To avoid the problems described above, the optical cavity was mounted within the vacuum chamber by being fixed to bracket mounts attached to the inside of two opposing 8” flanges. These 8” flanges were machined with a custom pattern of 1.33” flange mounts on them as can be seen in below.

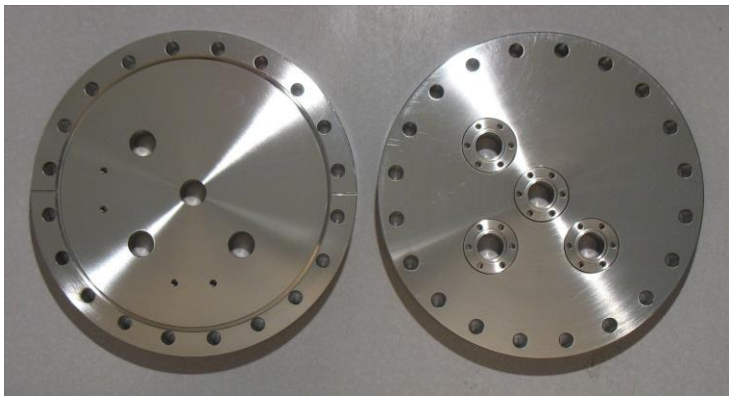

Figure 6.1 Custom 8” flanges: Left-interior face. Right-exterior face.

Mounted to the center of the flange is a 1.33” quartz viewport flange to allow an external light source to reach the internal cavity. Mounted on either side of the viewport and aligned with the optical mount adjusters are two rotary feedthroughs.

Figure 6.2 Rotary Feedthrough: Side view and End view.

The ends of these rotary feedthroughs were machined down to a flattened cross section and coupled into slotted brass fittings on the x and y tilt adjusters on the optical mount. This allows adjustment of the optical cavity while the chamber is sealed. There is a blank 1.33” flange on the last flange mount aligned with the third adjuster on the optical mount to allow for future expansion of the CEAS work to include adjustment of the cavity length for high resolution CRDS.

Figure 6.3 Optical mount with slotted brass fittings to be anchored within the chamber.

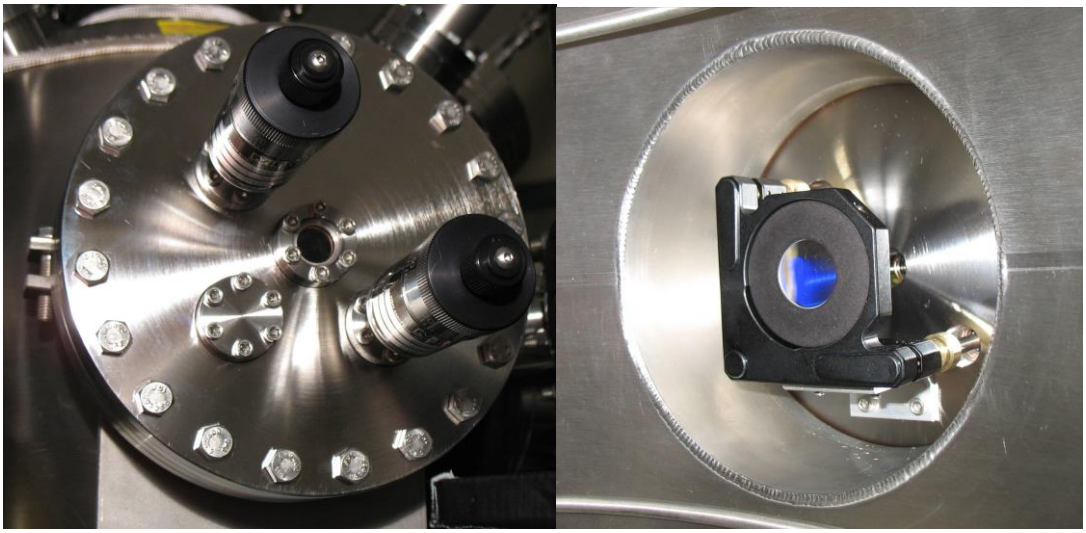

Figure 6.4 Fully assembled and installed optical setup in vacuum chamber (External adjustments and Internal Optics on one side).

Preliminary Light Source System

The light source used for initial testing of the cavity stability was a 635 nm red laser diode. A combination controller able to vary the laser's output power and maintain the diode temperature at a user defined level controls the laser diode. The temperature is maintained by adjusting the current to a thermoelectric junction mounted inside the diode mount assembly. There is also a collimating lens incorporated into the diode mount to focus the laser diode output into a useful beam.

While the cavity system, when on the optical table, can be adjusted to align the near mirror's optical center with the incident beam, the cavity contained in the vacuum chamber cannot because both mirrors are fixed to stationary flanges. To account for this, the incident beam location and direction must be adjustable. The solution to this problem was to mount the diode laser on optical

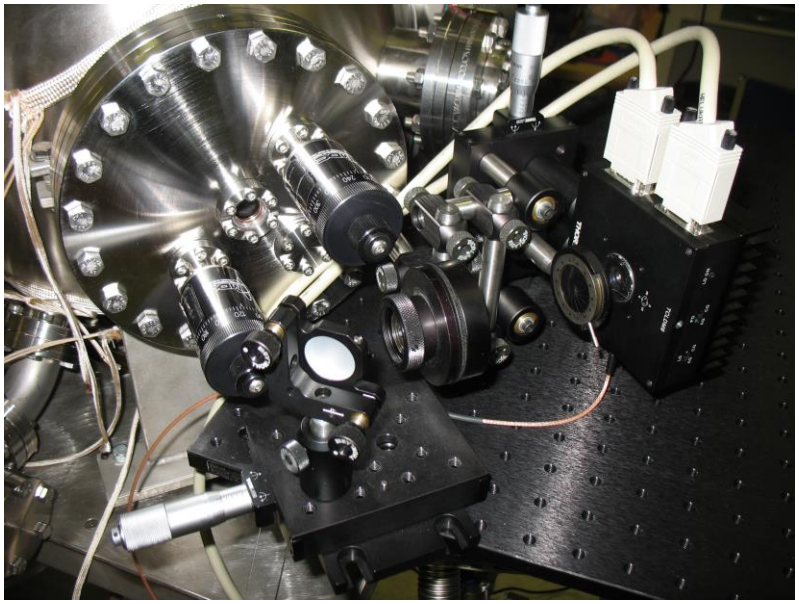

Figure 6.5 Diode mount and mirror assembly.

breadboard attached to the vacuum chamber cart. This breadboard holds the laser diode mount, two adjustable iris apertures, and a plane turning mirror mounted in an adjustable optical mount. The laser diode mount was mounted on a vertical translation stage that would allow for vertical alignment of the laser beam with the optical center of the input mirror. The adjustable optical mount with the plane mirror is on a post and holder assembly on a horizontal translation stage oriented such that the movement of the translation stage is along the direction of the laser beam. This mirror can then be adjusted to direct the beam straight into the optical cavity, and then the stage adjusted until the beam is aligned laterally with the input mirror's optical center.

This configuration produced inconsistent ringdown measurements, and it was recognized that the end of the vacuum chamber cart with the optical breadboard attached to it was capable of flexing and vibrating. To rule out any mechanical vibrations this may introduce, a large angle iron bracket was

designed and machined to hold the optical elements pictured above. This bracket, picture below, fastened directly to the vacuum chamber and would eliminate any vibrations that might be experienced independent of vibrations the entire chamber might experience.

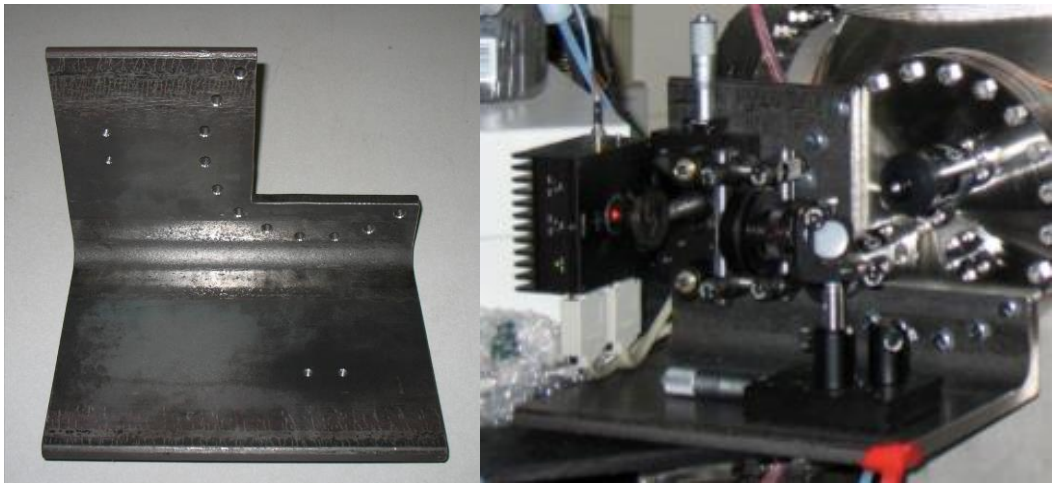

Figure 6.6 External Optics Bracket: with and without diode system installed.

With this addition, it was reasonable to conclude that mechanical vibrations would no longer be a significant source of signal noise. Using relatively rudimentary software that was able to read the ringdown waveforms from the oscilloscope to a PC and provide a reasonable approximation of the ringdown time as a function of elapsed time, it became evident that the quality of laser diode itself coupled with the weaker absorption cross section of O_3 at 635 nm was the source of the problem. Even with mirrors with 99.98% reflectivity, one standard deviation, equal to 2.76% of τ_0, corresponded to a 772 ppb variation from the average value.

Light Source Currently Being Utilized

This indicated a need for both a more stable laser system and a laser whose output is at a wavelength with a higher absorption cross section. The

cross section for O_3 at 635 nm is 3.26×10^{-25} cm^2 [11]. As was stated earlier, O_3 is a very strong absorber in the Hartley-Huggins band from 210 nm to 310 nm. The fourth harmonic output of a Neodymium-doped yttrium aluminum garnet (Nd:YAG) laser is at 266 nm. The absorption cross section for O_3 at this wavelength is 9.38×10^{-22} cm^2 [11] which represents a significant increase. A small pulsed Nd:YAG laser was available and was incorporated into the system, replacing the diode laser module. In contrast, once this laser was integrated into the existing system, using cavity mirrors that were only 99.7% reflective, one standard deviation from average was equal to 1.6% of τ_0, the corresponding error in concentration is only 6.01 ppb. The reason for this drastic difference lies in the increased absorption coefficient, because changes in concentration now generate large changes in ringdown time. This in turn minimizes the effect of noise in the signal.

Using this laser system also simplified the ringdown data collection because there was no longer a need to trigger the cw diode laser off once a particular cavity output intensity was reach. The power supply of the 20Hz pulsed laser was capable of simultaneously sending a 5 volt TTL pulse to trigger the oscilloscope. Below is a picture of the laser input system as it was configured for the remainder of this project.

It can be seen that there are a number of new elements required to successfully guide the laser pulses into the optical cavity. The 266 nm UV laser pulse is powerful enough that some of that energy must be dissipated before it reaches the cavity optics.

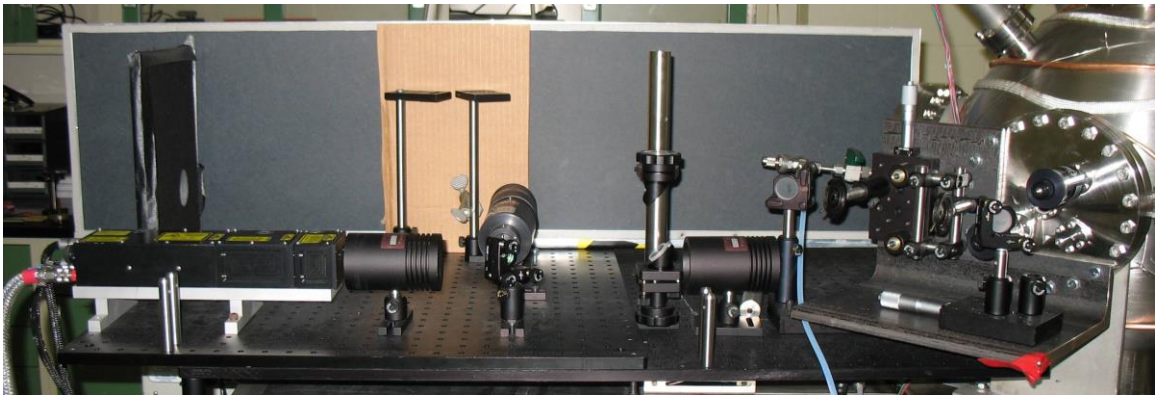

Figure 6.7 Nd:YAG laser and optical components that guide the laser pulses into the optical cavity.

To accomplish this, the first turning mirror in the vertical shift apparatus is actually a mirror designed for 532 nm reflectivity. This allows a significant portion of the UV light to pass through and into another beam dump, but the surface still reflects enough of the UV light up to the second turning mirror. Because the fundamental and second harmonics (infrared 1064 nm and green 532 nm, respectively) are also generated by the laser but not being utilized, a beam dump is placed near the laser output to safely disperse the majority of the energy from those wavelengths. Some of the light from those two wavelengths also coincides with the 266 nm UV laser pulse. The remaining three turning mirrors are specifically designed to reflect 266 nm laser pulses and act as filters by not efficiently reflecting the other two wavelengths. Aside from these differences, the general operating principle is the same as it for the 635 nm red laser diode.

Measurement and Data Collection Devices

While previous work had used a photo diode detector, a photomultiplier tube (PMT) was used to measure the cavity output intensity for this research. The PMT assembly shown below is comprised of a side exposure PMT in the

rectangular housing and a series of filters in the optical tube assembly.

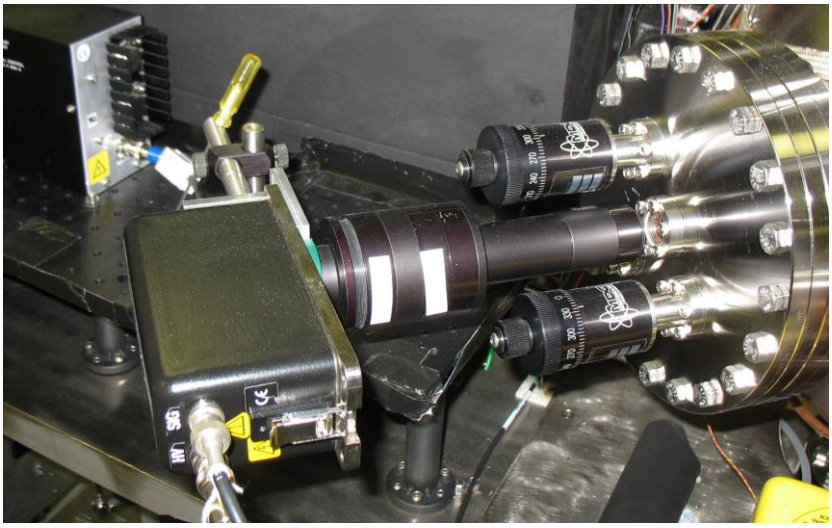

Figure 6.8 PMT Assembly.

In order going from the chamber to the PMT (right to left in the picture) there is a length of empty 1” tube, a 1” to 2” adapter, a 2” diameter optical density (O.D.) 1 neutral density filter, a 2” diameter O.D. 0.7 neutral density filter, another 2” diameter O.D. 1 neutral density filter, a 2” diameter bandwidth filter centered on 280 nm +/- 12.5 nm, a 2” to 1” adapter, and a piece of frosted quartz.

The empty section of 1” tube aids in alignment to ensure that, with all of the 2” filters (which do not fit between the rotary feedthroughs), the face of the PMT is still inline with the cavity output. This also helps prevent stray light from reaching the PMT photocathode.

In general, using neutral density filters to reduce signal intensity is not the preferred method to prevent detector saturation and/or damage as it can create signal to noise issues. If the PMT signal has random noise variations generating apparent fluctuations about the actual signal intensity, filtering half the light out would then make the same noise fluctuations twice as big relative to the signal.

One alternative method, which was used here, is to reduce the driving voltage to the PMT. This helps prevent saturation, and the power supply for the PMT used in this project was set at a 700 VDC output which is nearing the lower limit of linear behavior for the PMT used. Another common method to reduce signal intensity without necessarily affecting measurement noise is to reduce the input intensity. While this Nd:YAG laser system power supply does allow the user to adjust flash lamp intensity as well limit the amount of time allowed for the laser pulse to build, both of which result in an output intensity reduction, the laser was tuned and calibrated and its output is most stable when running near the maximum values. As was stated before when discussing the need to protect the cavity optics, the input beam was reflected off of a mirror designed for green light (532 nm) which greatly reduced the UV intensity reaching the optical cavity.

Even though these other methods were used, some filtering was still necessary to avoid saturating the PMT. A slight amount of intensity noise in measurements for ringdown is less of an issue that for standard absorption spectroscopy because the measured quantity is the time dependence and not the overall intensity. That does not mean this experimental method is noise immune. It just means that a small amount of noise can be averaged out without a large loss in data resolution.

The optical bandwidth filter aids in preventing external light or any residual 532 nm or 1064 nm light from reaching the PMT face. In very low levels, this would introduce a vertical offset to the ringdown waveform, but significant levels of any light can contribute to PMT saturation or even damage. The frosted

quartz intentionally has minimal affect on overall signal intensity. It is in place to diffuse the light reaching the PMT to avoid high intensity spots overexciting small regions. With all of the elements in front of the PMT face, the overhead lights in the lab do not generate any signal offset.

Sliding Radiation Source Cover

It also became evident, as will be pointed out in the results section, that a method to cover and uncover the radiation sources without opening the vacuum chamber was needed to get useful results. To accomplish this task a pneumatic linear feedthrough, pictured below, with 2” of travel was installed.

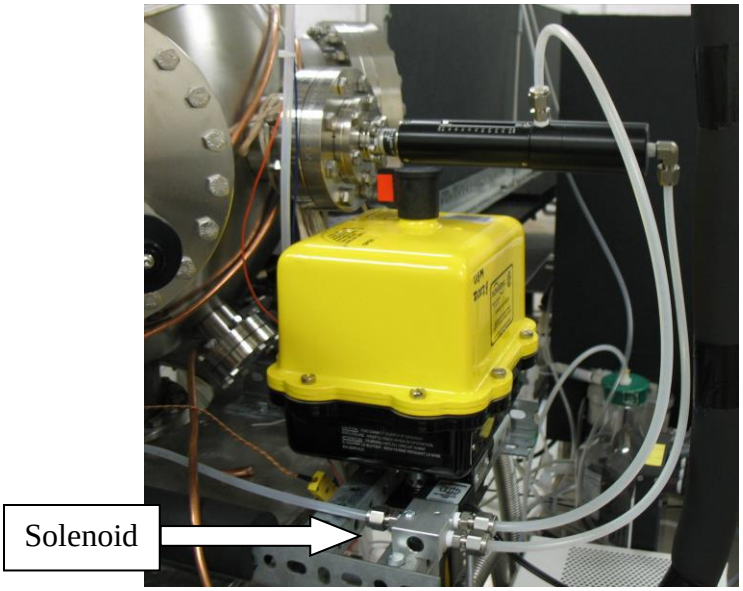

Figure 6.9 Pneumatic Linear Feedthrough before installation (above) and Linear Feedthrough after installation with pneumatic control lines and solenoid control valve (below).

An aluminum fixture extends the reach of the piston while a small section of an aluminum plate is attached to slide back and forth to cover and uncover the sources as can be seen below in the open and closed positions. Also within the chamber is a piece of aluminum stock that was milled out to accommodate the ^{210}Po sources either one or two at a time. This allowed the aluminum plate to slide over the sources without disrupting the alignment or pushing them off the central platform. This component also ensures that the sources go back into the same position each time to create a more reproducible procedure.

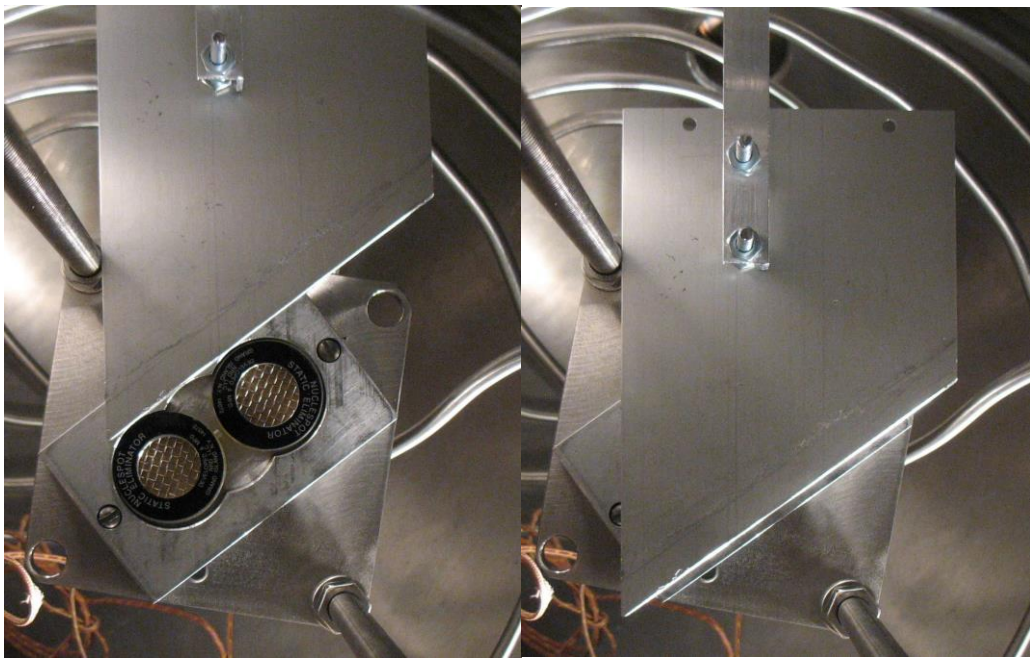

Figure 6.10 Sliding aluminum source cover shown opened (left) and closed (right).

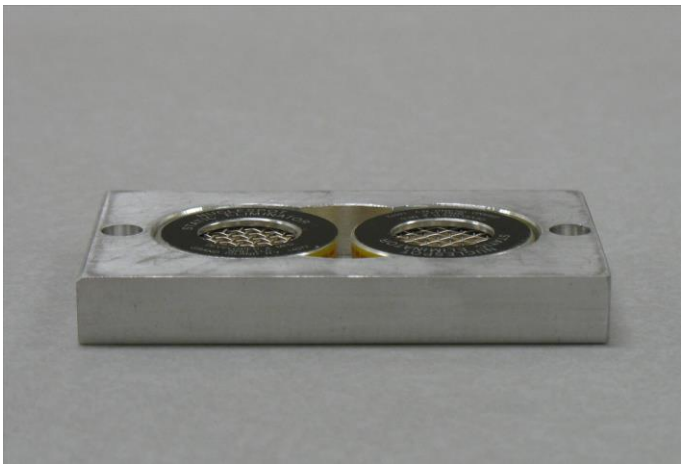

Figure 6.11 ^{210}Po Sources in the Aluminum Holder.

The pneumatic device is actuated by a 4-way solenoid valve that is controlled in conjunction with the software developed to run this experiment (discussed in the next section). This solenoid valve ensures that the arm is either all the way extended or all the way retracted when adequate air pressure is supplied to the pneumatic line.

Flow Through Capability

As mentioned earlier, a number of studies involving the measurement of chemicals produced by radiation used flow chambers. These publications reported increased product yield in flowing systems. A flange with two shut off valves, shown below, has been installed that allows for flow through the vacuum chamber. The gas is mixed in the previously discussed multi-tube mixing regulator, and flow is introduced through the existing manifold. This allows for gas movement through the area being exposed to radiation.

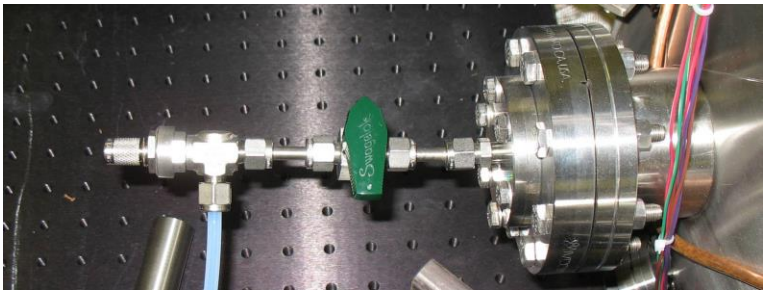

Figure 6.12 Flange allowing flow output from chamber with redundant shut off valve (shown with shut off valves closed).

Also, all non-metallic tubing is made of Teflon, and Teflon tee junctions allow two commercial O_3 analyzers to pull gas samples before the gas enters the manifold and after it exits the chamber. With the mercury lamp device installed inline just after the multi-tube regulator, the system has the ability to generate O_3 and measure its concentration via the analyzers as well as CRDS. While the metallic surfaces as well as other chemical species will contribute to the decomposition of O_3, it will be considered a confirmation of general accuracy if the CRDS measurement is between the two analyzers' measurements.

CHAPTER VII

SOFTWARE DEVELOPMENT

Initial ringdown data was collected using the digital oscilloscope's internal save function. This saved individual wave forms to a 3 ½" floppy disc. The waveforms files were .csv files containing two columns of numbers: time and voltage. These then needed to be analyzed by plotting them on a computer and, using a data analysis program such as Sigma Plot, fitting an exponential function to the data set. The exponential coefficient in the function provided the ringdown time, τ, from which the desired information could be extrapolated (reflectivity, concentration, etc.). This method is very reliable and works well for stable sample gases and measurements that are not very time sensitive. On the other hand, even if one saves multiple waveforms to evaluate changes in concentration, one can only evaluate a qualitative time evolution because this lacks a reliable measurement of time between measurements.

To be able to quantitatively evaluate any time dependence of the radiation's affect on the atmosphere within the vacuum chamber, it was necessary to monitor the PMT signal on every laser pulse. A National Instruments (NI) PXI data acquisition system with a digitizing module was available and replaced the oscilloscope for reading the PMT output voltages. This alternative to the oscilloscope connected to a computer via a pair of Ethernet cables and is capable of continuously streaming data from the PMT to the computer. Having switched to a data collection device that did not have any inherent data handling capabilities, it became necessary to write a new program

to aid in evaluating cavity alignment as well as measure and record data. This new program would also need the ability to control the new linear motion feedthrough to cover and uncover the sources in the chamber.

Eventually four programs were written to provide the necessary system controls, feedback, and measurements. The programs were written in a graphical programming language created by NI called LabVIEW (Laboratory Virtual Instrumentation Workbench). There are two programs used to evaluate the cavity's alignment as well as stability and record various data sets. Another program was written that uses an automated sequence to cycle the vacuum system between 760 Torr and < .01 Torr multiple times, alternating between ultra high purity (UHP) N_2 and dry air. The other program written for this project indicates chamber pressure and provides basic controls of the vacuum system components required to cycle chamber pressure.

The program used in tuning the cavity alignment titled "Ringdown Alignment Assist.vi" provides the user with several different useful values to aid in achieving a reliable ringdown measurement. As can be seen in the screen shot on the next page, this program displays a full view of the ringdown waveform in the upper left section of the screen. This waveform is displayed with a 20-sample running average which is equivalent to a one second average for the 20 Hz laser pulse input, and all other data operations are performed on this averaged waveform. In the upper right section there are two plots showing two different regions of the ringdown decay. Each of these is shown with an exponential decay curve overlaid that is a fit calculated over the region displayed. These regions are

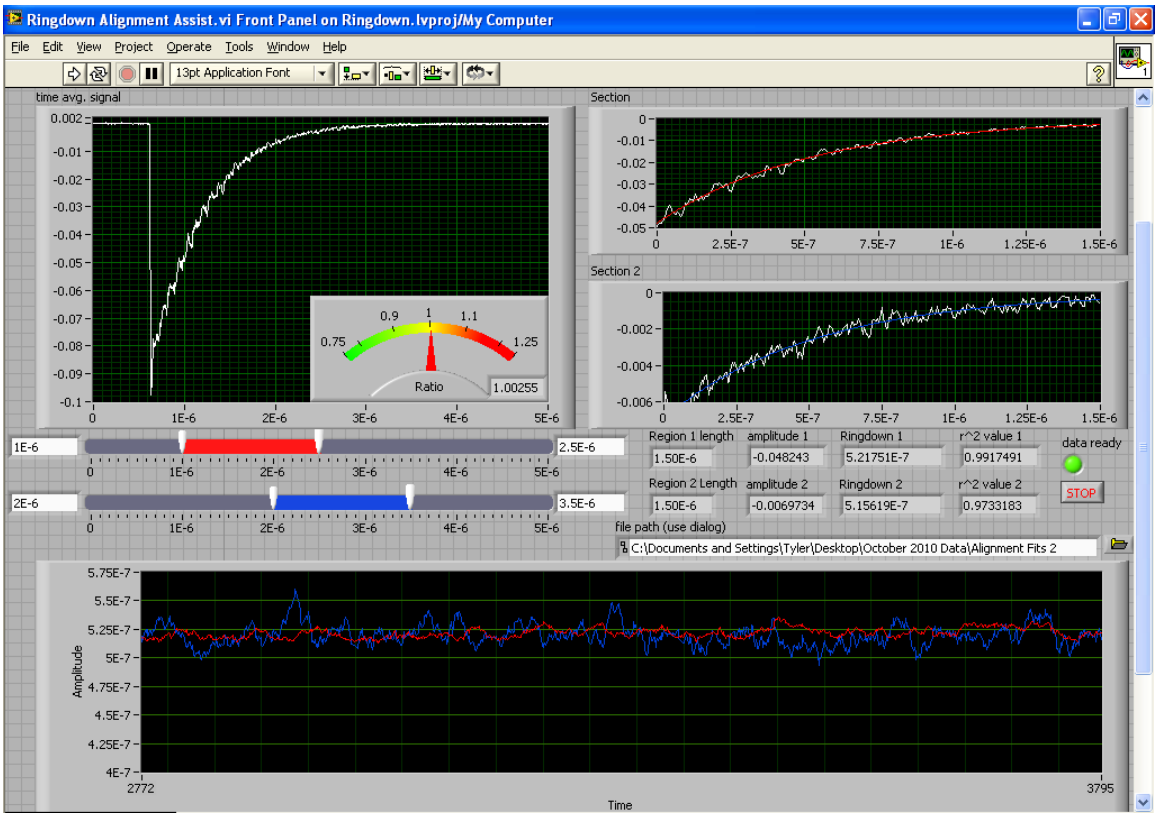

Figure 7.1 The front panel for Ringdown Alignment Assist.vi (above) and the corresponding block diagram (below) as an example of the LabVIEW programming language.

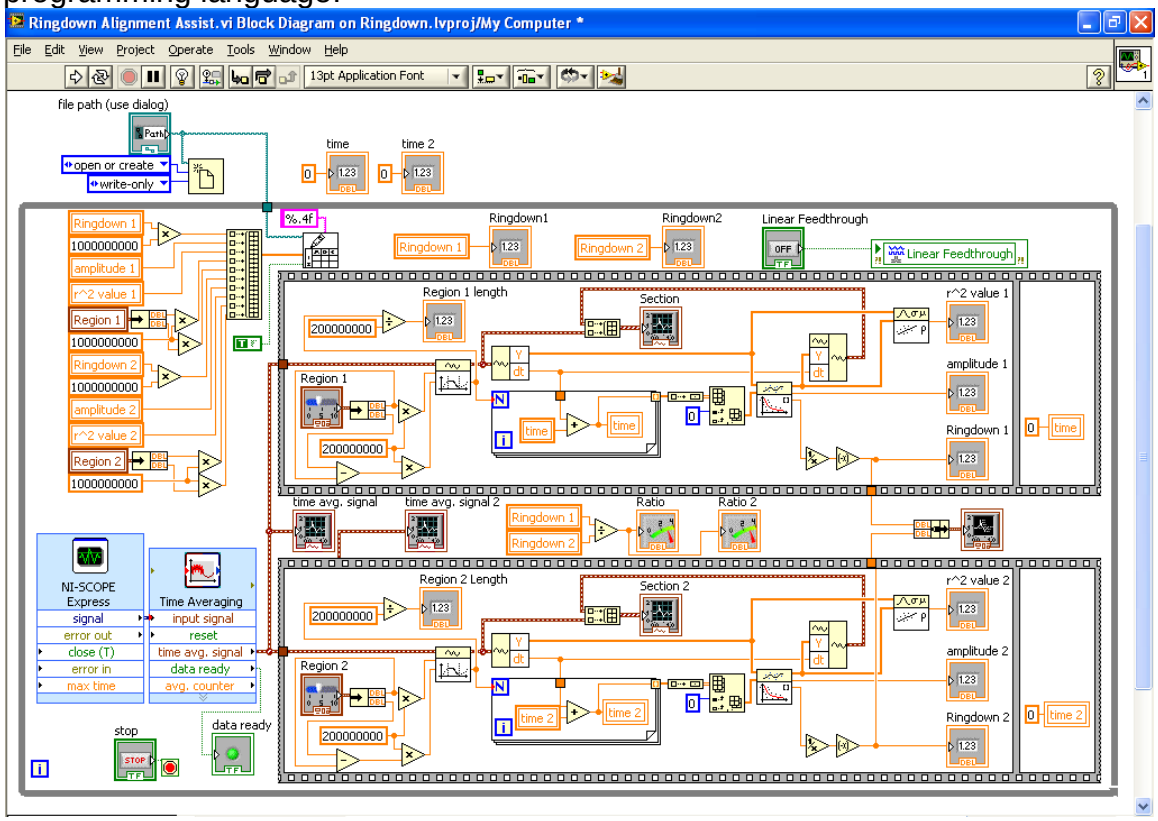

user defined by the red and blue sections marked the sliders below the ringdown waveform and can also be adjusted by typing in numerical values at either end of the slider area. The ringdown times calculated over each region are shown in the chart at the bottom of the screen. The values corresponding to each fit are also displayed in the numerical indicators in the middle of the screen on the right. All of these values with the exception of the region lengths (region boundary values are recorded instead) are recorded in a text file whose name and location are defined by the user. A ratio of the two ringdown time values is also provided as well as a meter to provide a quick visual reference. This ratio is used to identify when the cavity is excited in a manner that yields a high quality single exponential decay. When the cavity is not appropriately aligned, the ringdown curve may not match a single exponential shape. Once the cavity is adequately aligned, this virtual instrument (VI) is stopped, and “Ringdown Time.vi” is started.

“Ringdown Time.vi” is the VI that collects the experimental data corresponding to events of interest. The waveform data in this VI is also averaged over 20 samples, but it is a block average as opposed to the running averaged used during the cavity alignment process. User controls and inputs in this VI include defining the fit region length and start time, how long the τ_0 value is averaged, when a waveform is saved, whether the sources are covered or uncovered, the length of the optical cavity (d), the absorption cross section of the gaseous species expected to be produced, when to put a ‘mark’ in the data file, and the filename and location for the three data files: saved waveforms, overall ringdown information, and calculated concentration information. This VI

calculates a running average of τ_0 as long as the “Run tau0 Average” button is selected which is displayed as a red line on the chart in the lower left portion of the screen. While this average is being calculated, the standard deviation, maximum, and minimum values are also being calculated as well as the calculated concentration values corresponding to one standard deviation based on the cavity length and absorption cross section values provided. Once this button is deactivated, that row of values is set to provide a reference while the experiment is running, and running concentration value is calculated in number density and ppb with the ppb values being displayed on the chart at the lower right portion of the screen. Based on τ_0 and the cavity length, the effective mirror reflectivity is also calculated.

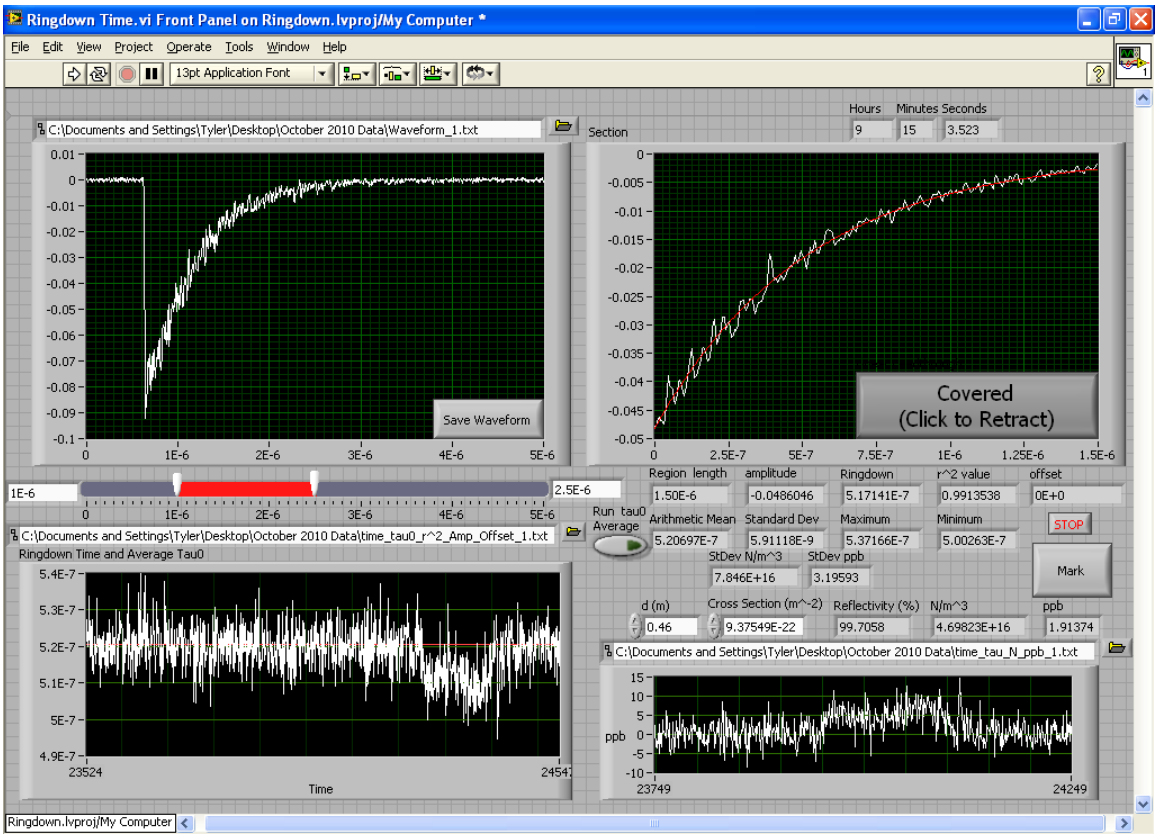

Figure 7.2 Front Panel for Ringdown Time.vi with representative data displayed.

The program written to cycle between vacuum pressures and alternating UHP N_2 and dry air allows the user to define how cycles are desired and the amount of time spent at each pressure. The user also defines what to name the file recording chamber pressure and temperature. All of these values must be entered before the VI is started. Once started, numerical indicators arranged vertically near the center of the screen provide the temperatures of the chamber wall and atmosphere, the chamber pressure is indicated by the appropriate capacitance manometer depending on whether the pressure is above or below 1 Torr, and the number of cycles completed. On the right, green 'LED' indicators (all shown off) provide the user information concerning the current status of system components. The indicators located along the bottom of the screen allow the user to see what phase of the cycle the system is in and how long it has been in the current phase.

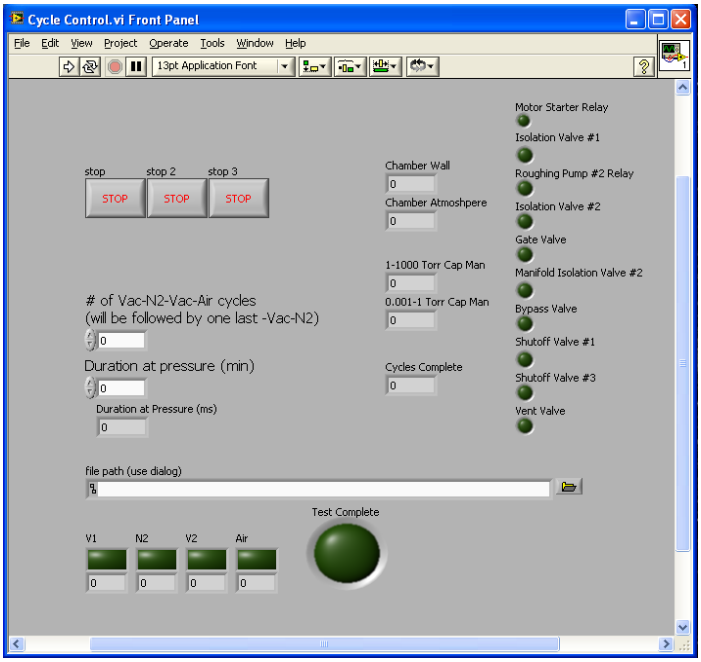

Figure 7.3 Front Panel for "Cycle Control.vi."

When not running sequential vacuum cycles, a simple program title “Basic Controls.vi” was used to allow for system manipulation. It contains a list of user controls and the capacitance manometer pressure indicators. It included only the controls necessary to evacuate the chamber pressure and back fill it with either UHP N_2 or dry air as well as a control to open and close the vent valve and a control to cover and uncover the sources.

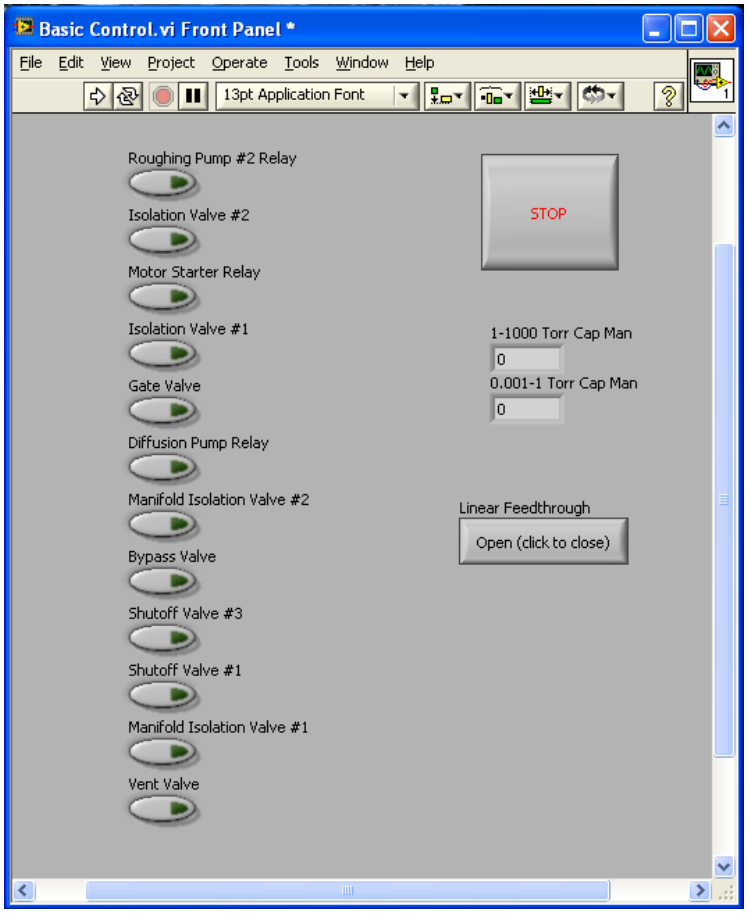

Figure 7.4 Front Panel for “Basic Control.vi.”

CHAPTER VIII

DATA COLLECTION AND RESULTS

Once the system and the software were capable of measuring and recording ringdown data, the first step was to check to see if the ringdown measurent was stable in static conditions as well as throughout pressure cycles from ~760 Torr to below one Torr and back. The chart below shows a series of pressure cycles alternating the backfill gas between UHP N_2 and dry air. Also provided is a chart showing average ringdown values while at each pressure. The shift in ringdown time between measurements taken at ~760 Torr and ~.115 Torr is consistent with the expected difference from Rayleigh scattering due to

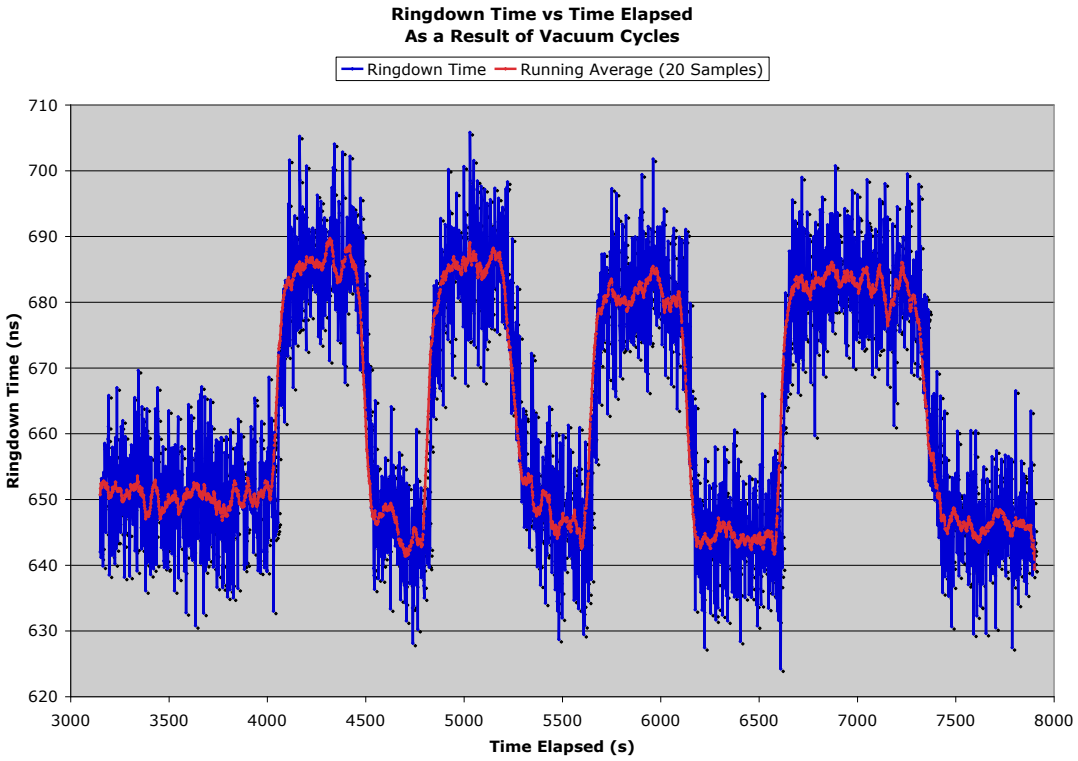

the presence or absence of gas in the chamber [18, 19].

Figure 8.1 The plot above shows ringdown time vs elapsed as affected by pressure changes. Prior to these cycles the chamber was held at its lower limit by the diffusion pump to allow the interior to outgas as much as was possible.

Table 8.1 The Averaged Ringdown Values Corresponding to Each Phase of the Cycle

Cycle Number	Ringdown Time at ~115mTorr (ns)	Ringdown Time at ~750 Torr UHP N_2 (ns)	Change in Ringdown Time (ns)	Predicted Shift Due to Rayleigh Scattering (ns)
		650.3		
1	686.38	645.23	41.15	33.49
2	685.7	647.8	37.9	32.81
3	681.92	644.31	37.61	33.07
4	682.83	649.57	33.26	33.16

This confirms that the initial goal has been achieved. The system is capable of continuously measuring ringdown values even through extreme pressure variations. The ringdown times are reproducible after several pressure cycles. The next step was to evaluate the system's ability to measure O_3 accurately by using the multi-tube flow meter, mercury lamp, and O_3 analyzer system previously mentioned. After letting UHP N_2 flow through the chamber to establish a τ_0, a 10% dry air mixture balanced with UHP N_2 was exposed to the mercury lamp before being analyzed by the first O_3 analyzer and then flowing through vacuum chamber system. Flowing through the chamber allowed the ringdown system to measure the change in ringdown time due to O_3 absorption, and the second analyzer measured the concentration in the chamber exhaust line before it was scrubbed by the steel wool filter. The first analyzer confirmed a significant amount of O_3 was entering the vacuum system manifold (~1385 ppb), but as expected, the value reaching the chamber and second analyzer was greatly reduced because of the reactive material (metal) in the vacuum chamber

and air's natural tendency to convert the O_3 back to O_2. Shown below is a plot of O_3 concentration measured both by the ringdown system and the second analyzer. The discrepancy in the rising edge can be attributed to the diffuse mixing that occurs as the gas mixture flows out of the ¼" steel tubing and into the 18" diameter chamber. However, it is evident that as the gas mixes more thoroughly as time passes, the analyzer and CRDS values are in close agreement. Once the mercury lamp is turned off and the mix is switched back to

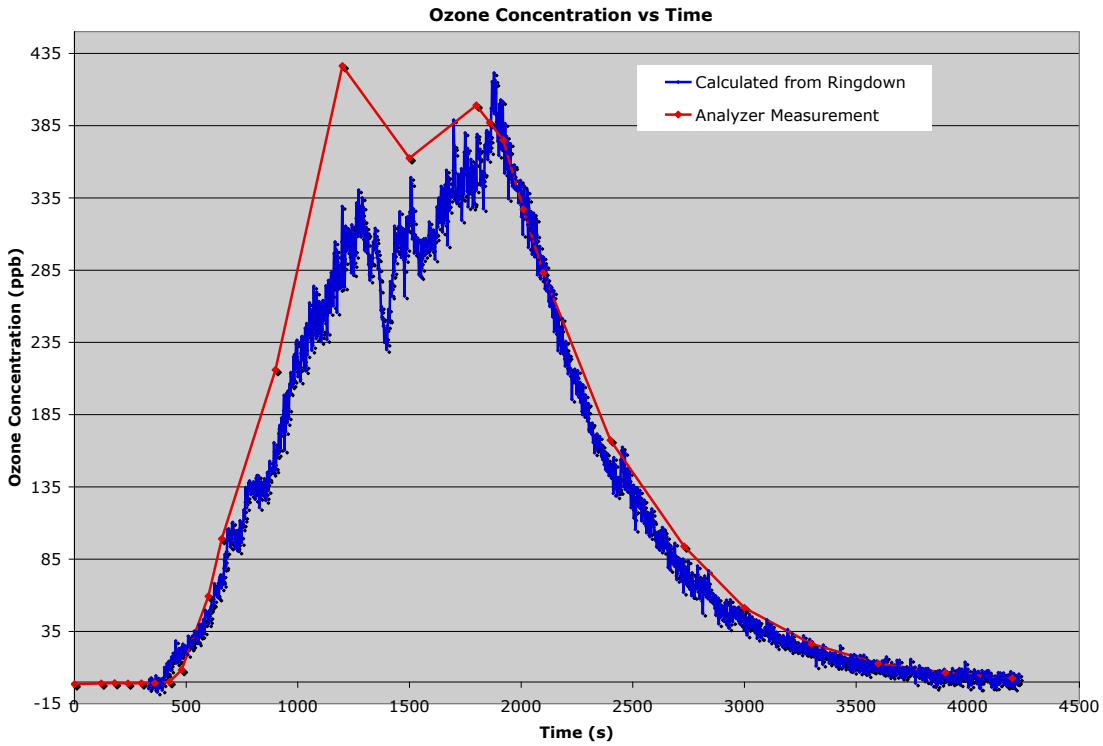

only UHP N_2, it can be observed that the two measurements are very consistent in measuring the drop in O_3 concentration.

Figure 8.2 Demonstrating the ringdown system's ability to accurately measure O_3.

With the system confirmed stable and capable of measuring O_3, the next step was to devise a plan to evaluate its ability to detect chemical products

generated as a result of atmospheric gasses being exposed to an alpha radiation source. One issue that was discovered was that it took approximately one minute and twenty seconds for the chamber pressure to transition from less than one Torr to 760 Torr. However, the production of O_3 from a high energy electron beam passing through a N_2-O_2-H_2O system had previously been observed to be a quick process and short lived process. The O_3 concentration changed rapidly and was seen as an intermediate step in the production of other chemical products [10]. Thus, a rapid method of exposing or shielding the sources was necessary. This was the reasoning for developing the sliding cover system that was installed. Once this was installed, one then had the ability to cover the sources, evacuate the system, backfill with air, and then cycle the cover opened and closed to test for any response in the ringdown time to the presence of absence of the alpha radiation. The figures on the following page show the ringdown time during such a test as well as the corresponding concentrations calculated from these ringdown time variations assuming the absorbing species is O_3.

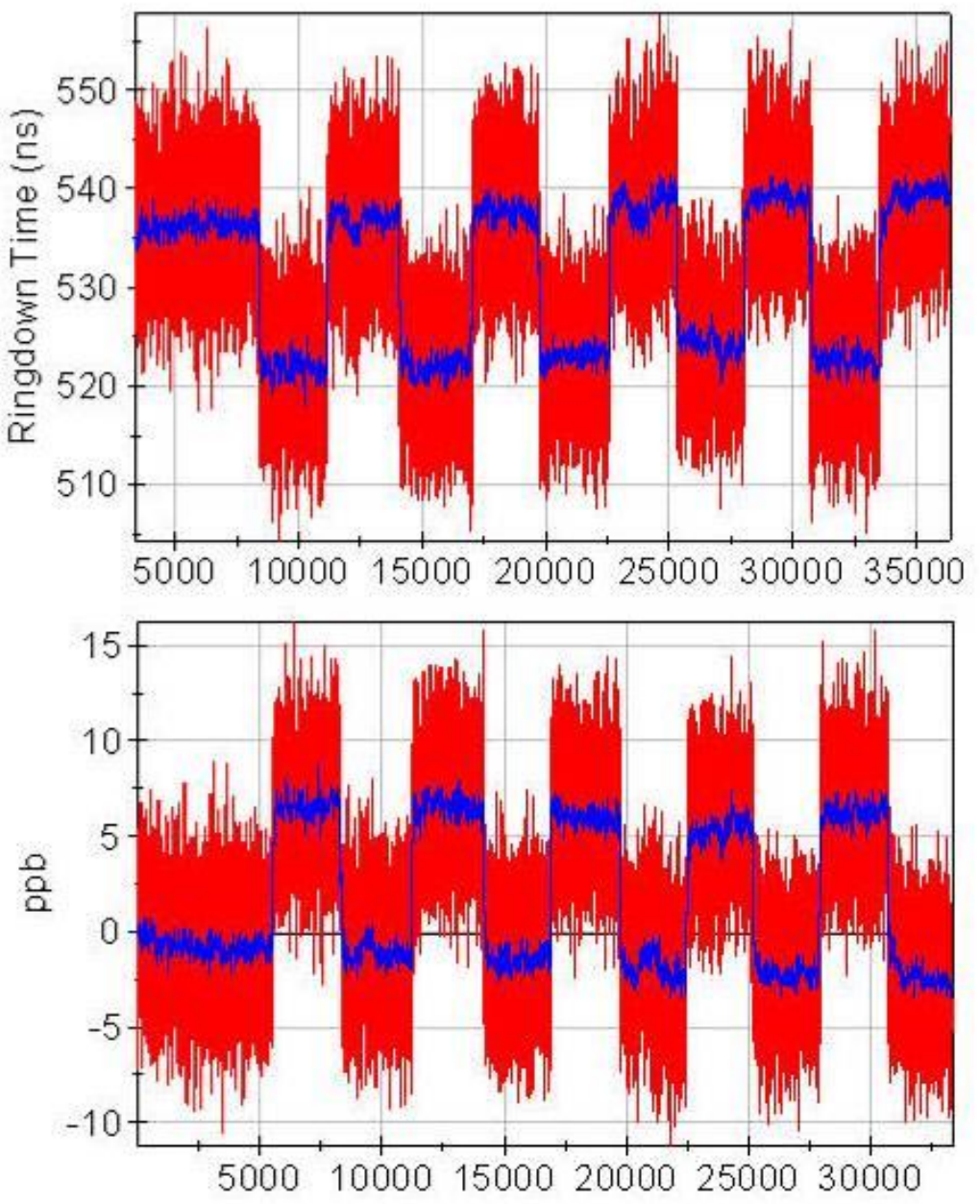

Figure 8.3 Ringdown Times vs Elapsed Time (Top) and ppb of O_3 vs Elapsed Time (Bottom) as affected by uncovering and covering the alpha sources.

CHAPTER IX

CONCLUSIONS AND FUTURE WORK

The consistent signal variation resulting from uncovering and covering the alpha sources is evidence that this system using CRDS is capable of detecting the effect of ionizing radiation from an alpha source on air inside the vacuum chamber. This had not yet been achieved using an optical detection method that was able to monitor concentrations of absorbers on the time scale over which they are produced. While it is well understood that O_3 is produced and has a strong absorption cross section at 266 nm, it can not be said conclusively that the only absorbing species produced in the experiment was O_3. The following chart provides the cross sections near 266 nm of other chemical species known to be produced by ionizing radiation and the concentrations that would be calculated if they were to be the sole absorber responsible the shift in ringdown time.

Table 9.1 Predicted Concentrations Resulting from the Observed Shift in Ringdown Time of Other Potential Products of Ionizing Radiation and Their Absorption Cross Sections

τ_0 = 536 ns		τ = 521 ns
Species	Absorption Cross section (cm^2)	Concentration
O_3	9.38E-22	7.78 ppb
N_2O_5	1.77E-23	412.32 ppb
NO_3	1.20E-23	608.17 ppb
NO_2	3.85E-24	1895.59 ppb
N_2O	3.50E-29	208515131.7 ppb

While the necessary concentration to achieve an equivalent absorption for N_2O is unreasonable, the other values are not necessarily unachievable. It is likely that while O_3 may be responsible for most of the observed effect, some other species may contribute. A combination and not just one of the absorbers may be present. Future work on this topic could include using at least four other wavelengths, each wavelength at a large absorption cross section for a different chemical species. This would create a system of equations that would allow one to calculate the concentrations of each of these absorbers. With the hardware infrastructure developed through this research, using a different wavelength would only require an appropriate light source, mirrors for that particular wavelength, and a different filter on the PMT.

These measurement capabilities would also allow for the introduction of other gasses (water vapor, increased CO_2 levels, etc.) to simulate a variety of atmospheric conditions. The fact that this CRDS system is integrated into a vacuum chamber would also allow for the simulated atmospheric compositions to also be simulated at a variety of altitudes. From there one could examine any number of phenomena from continued exploration of chemical production to the effects of increased ion concentration in the presence of water vapor. There are several different research opportunities created by the versatility of the vacuum system combined with the real time CRDS measurements.

REFERENCES

[1] L'Annuniata, Michael F.; *Radioactivity: Introduction and History*; Elsevier: Amsterdam, The Netherlands, 2007; Page 1.

[2] Miller, Dudley G.; *Radioactivity and Radiation Detection*; Gordon and Breach Science Publishers: New York, NY, 1972; 1-36.

[3] Berger, M.J.; Coursey, J.S.; Zucker, M.A.; Chang J.; *Stopping-Power and Range Tables for Electrons, Protons, and Helium Ions;* http://www.nist.gov/pml/data/star/index.cfm; For values pertaining to dry air (retrieved on October 21, 2010).

[4] Hubbell J.H.; Seltzer, S.M.; *Tables of X-Ray Mass Attenuation Coefficients and Mass Energy-Absorption Coefficients*; http://www.nist.gov/pml/data/xraycoef/index.cfm; For values pertaining to dry air (retrieved on October 21, 2010).

[5] Heicklen, Julian; *Atmospheric Chemistry*; Academic Press: New York, NY, 1976; 3, 58-64, 274-277, 304-306.

[6] Environmental Protection Agency; Air Quality Criteria for Nitrogen Oxides; *Air Pollution Control Office Publication No. AP-84*; Washington D.C., January 1971; Page 6-2.

[7] Lind, S. C.; Bardwell, D. C.; Ozonation and Interaction of Oxygen with Nitrogen Under Alpha Radiation; *J. Am. Chem. Soc.* **1929**, *51* (9), 2751-2758; (And References Therein).

[8] Armstrong, D.A.; The Radiation Chemistry of Gases; *Radiation Chemistry: Principles and Applications*; Farhataziz, Michael A. J. Rodgers; VCH Publishers: New York, NY, 1987; 263-319.

[9] Willis, C.; Boyd, A. W.; Young, M. J.; Radiolysis of Air and Nitrogen-Oxygen Mixtures With Intense Electron Pulses: Determination of a Mechanism by Comparison of Measured and Computed Yields; *Can. J. Chem.* **1970**, *48* (10), 1515-1525.

[10] Jones, A. Russell; Radiation-Induced Reactions in the N_2-O_2-H_2O System; *Radiation Research* **1959**, *10* (6), 655-663.

[11] Hannelore Keller-Rudek, Geert K. Moortgat, *MPI-Mainz-UV-VIS Spectral Atlas of Gaseous Molecules,* www.atmosphere.mpg.de/spectral-atlas-mainz; For O_3 absorption spectrum and molecular absortion values pertaining to 266 nm (retrieved on October 21, 2010).

[12] Paldus, Barbara A.; Kachanov, Alexander A.; An historical overview of cavity-enhanced methods. *Can. J. Phys.* **2005***, 83*, 975-999. (And references therein).

[13] Richards, W. G.; Scott, P. R.; *Structure and Spectra of Molecules*; John Wiley & Sons Ltd.: Hoboken, NJ, 1985; 93-94.

[14] Scherrer, Susan T. A Novel Diode Laser Cavity Ringdown Spectroscopy System for Trace Volatile Organic Compound Detection. Master's Thesis, Mississippi State University, Mississippi State, MS, May 2002.

[15] Yu, Wei Wen. Cavity Enhanced Methods For Trace Gas Concentration Measurements. Master's Thesis, University of Southern Mississippi, Hattiesburg, MS, August 2008.

[16] Buchanan, Aubri Capri. Characterization of Air Fluorescence Induced By Alpha Radiation. Master's Thesis, University of Southern Mississippi, Hattiesburg, MS, August 2008.

[17] Reese, Tyler W.; Winstead, Chris B.; Implementation and Manipulation of a Stable Optical Cavity within a Vacuum Chamber; Presented at the 55th International Instrumentation Symposium, League City, TX, June 2009.

[18] Jackson, John David; *Classical Electrodynamics*, Third Edition; John Wiley & Sons, Inc.: Hoboken, NJ; 466.

[19] Griesmann, U.; Burnett, J.H.; Refractivity of nitrogen gas in the vacuum ultraviolet, Opt. lett. 24, 1699-1701, 1999. (As referenced by http://refractiveindex.info/; refractive index of N_2 at 266 nm retrieved October 21, 2010).